# Experimental Design for Study of Nucleate Boiling in Porous Structures

by

Mitchell Joseph Kelley

Submitted to the
Department of Mechanical Engineering
in partial fulfillment of the
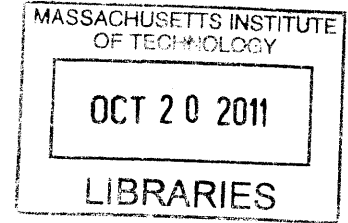requirements for the Degree of

Bachelor of Science

at the

Massachusetts Institute of Technology

June 2011

© 2011 Mitchell J. Kelley
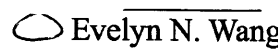
The author hereby grants to MIT permission to reproduce and to distribute publicly paper and electronic copies of this thesis document in whole or in part in any medium now known or hereafter created.
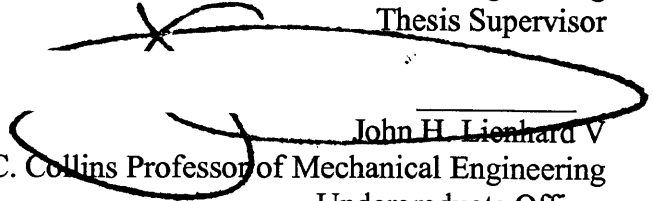
Signature of Author: _____

Department of Mechanical Engineering
May 24, 2011

Certified by: _____

Evelyn N. Wang
Esther and Harold E. Edgerton Assistant Professor of Mechanical Engineering
Thesis Supervisor

Accepted by: _____

John H. Lienhard V
Samuel C. Collins Professor of Mechanical Engineering
Undergraduate Officer

1

# Experimental Design for the Study of Nucleate Boiling in Porous Structures

by

Mitchell Joseph Kelley

Submitted to the Department of Mechanical Engineering
on May 24, 2011 in Partial Fulfillment of the
Requirements for the Degree of Bachelor of Science in
Mechanical Engineering

## Abstract

The superheat required to initiate nucleate boiling inside porous wicks is not well understood in practice. This thesis reports the design of an experimental setup for investigating the onset of vapor nucleation in sintered porous structures. Pressure sensing was evaluated as an effective means of detecting the onset of nucleation. Thermal studies were conducted with a custom finite difference script in conjunction with finite element analysis. Heat conduction through a three dimensional wick was reduced to one dimensional conduction via symmetry and design constraints. The wick was optimized to achieve a temperature drop of 30 °C at a common heat pipe operating temperature of 70 °C.

Thesis Supervisor: Evelyn Wang
Title: Esther and Harold E. Edgerton Assistant Professor of Mechanical Engineering

## ACKNOWLEDGEMENTS

I would like to thank my thesis advisor, Evelyn Wang, who welcomed into her Lab the summer of my sophomore year and immersed me in university research with a great team of students and professors on a project from which this thesis was inspired. I would like to thank Arthur Kariya for his perpetual support, enthusiasm, and high standards which contributed in a huge way towards making this project successful and rewarding. Thanks to the members of Professor Wang's Device Research Lab for the spontaneous advice and humor which make "going into lab" exciting during rough spots. And finally, a big thanks to my family and friends whose encouragement and heckling I couldn't do without.

# 1 Table of Contents

# LIST OF FIGURES

# List of Variables

$w_r$ = wick radius

$w_z$ = wick height

$w_{ratio}$ = ratio of wick height to wick radius

$w_{ratio}$* = optimal ratio of wick height to wick radius

$T_r$ = Temperature of wick at edge of bottom surface

$T_z$ = Temperature of wick at center of top surface

$T_{hot}$ = Temperature of hottest part of the wick.

$\Delta T$ = Minimum temperature drop from $T_{hot}$ to the surface of the wick in contact with the water gap

$T_{ratio}$ = Ratio of coolest axial to radial temperatures

UA = Overall heat transfer coefficient

$\sigma$ = Surface tension

$D_p$ = Difference between pressure inside and outside a vapor bubble

# 1 Introduction

Nucleate boiling is well studied for flat surfaces but there has been very little investigation into the onset of nucleate boiling in porous structures. For a long time it has been necessary to understand the nature of nucleate boiling off of flat surfaces; the design of devices ranging from nuclear power plant heat exchangers to counter-top crock pots has depended on the ability to predict and understand nucleation. Much research has been conducted in pool and pipe boiling. Presently, with developments in microelectromechanical systems (MEMS) and engineered surfaces towards such devices as heat pipes there is a need to understand how boiling takes place in porous media.

For nucleation, it is known that in order for a vapor bubble to form there must be enough local free energy change such that enough liquid can be vaporized to support a bubble with a radius equal to or less than the critical radius. Bubbles with radii above this radius have enough volume to support themselves and will grow indefinitely while bubbles with radii below the critical radius are overpowered by interfacial energy and collapse on themselves. Due to this energy barrier, boiling does not happen at the saturation temperature, but rather at a temperature above the saturation temperature. The difference is called the superheat, which for water at atmospheric pressure ranges from 1 to 10 °C depending on the surface roughness.

For nucleation in a porous structure, a similar energy barrier exists, as well as a critical radius. However, if the effective pore size of the structure is less than the critical radius, the maximum size of the bubble will be limited to the pore size, and nucleation may be prevented. This thesis will report the design of *an experimental setup for investigating the onset of vapor nucleation in sintered porous structures.*

## 1.1 Application: Heat Pipes

The field with the most immediate need for an understanding of nucleate boiling in porous media is the heat pipe industry. Heat pipes are among the most efficient means of transferring heat. They are more effective than conduction through copper or diamond. Heat pipes can be made from inexpensive, low conductivity materials and still give high heat transfer performance because they transfer heat via phase transitions, similar to refrigeration systems.

Unlike refrigeration systems, heat pipes require no external energy supply to drive the flow. Fluids are circulated by capillary pressure alone.

Heat pipes transfer heat by utilizing the latent heat of phase change. The simplest form of heat pipe is a pipe capped at both ends with a porous wicking material coating the inside. The pipe is evacuated and filled with the working fluid, which is typically water for the temperature range of 20-300 °C. During operation, one end of the heat pipe is placed in a cool region (condenser), the other in a hot region (evaporator). Liquid water in the hot side vaporizes off the surface of the wicking structure and flows to the cool region of the heat pipe where it is condensed. The liquid returns from the cool condenser to the hot evaporator section by flowing through the wicking structure. The wicking structure supplies the capillary pressure required to pump the working fluid, pushing the vapor and pulling the liquid. The strength of the capillary pump is inversely proportional to the structure's pore size.
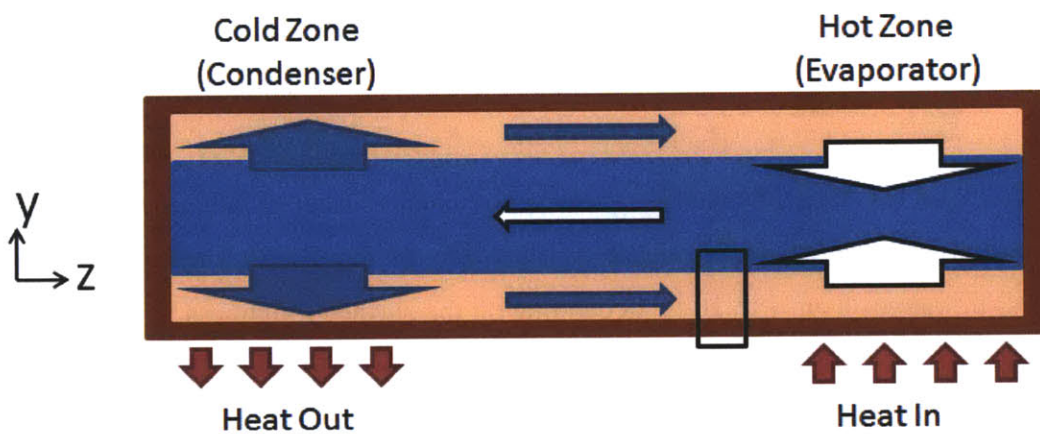


Figure 1.1: Heat pipe axial cross section indicating directions of vapor flow (white arrows) and liquid flow (blue arrows). (Zoom box featured in Figure 2.)
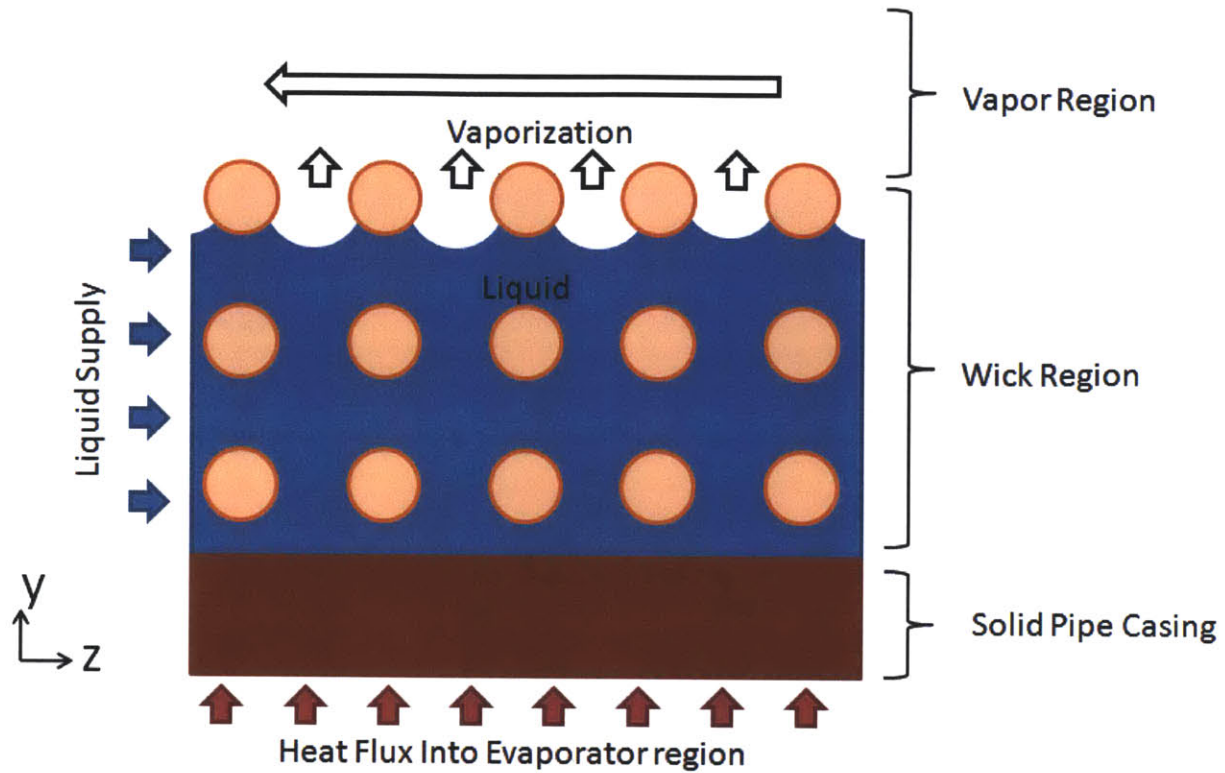
*Figure 1.2: Close up of heat pipe evaporator region as shown in Figure 1.1. Under normal operating conditions there is a steady supply of liquid balanced by steady evaporation at the upper surface of the wick. Here the wick structure is idealized as an evenly spaced matrix of spheres.*

Dry-out is a failure mode of concern. Under normal operating conditions, water vaporizes at the top of the wick as shown in Figure 1.2. If the evaporator is heated too rapidly, then it is possible for a vapor bubble to form inside the wick and rupture the meniscus that is driving the flow. In this event, the evaporator's supply of liquid water will be less efficient and may possibly fail due to complete constriction. Figure 1.3 illustrates the dry-out failure mode.
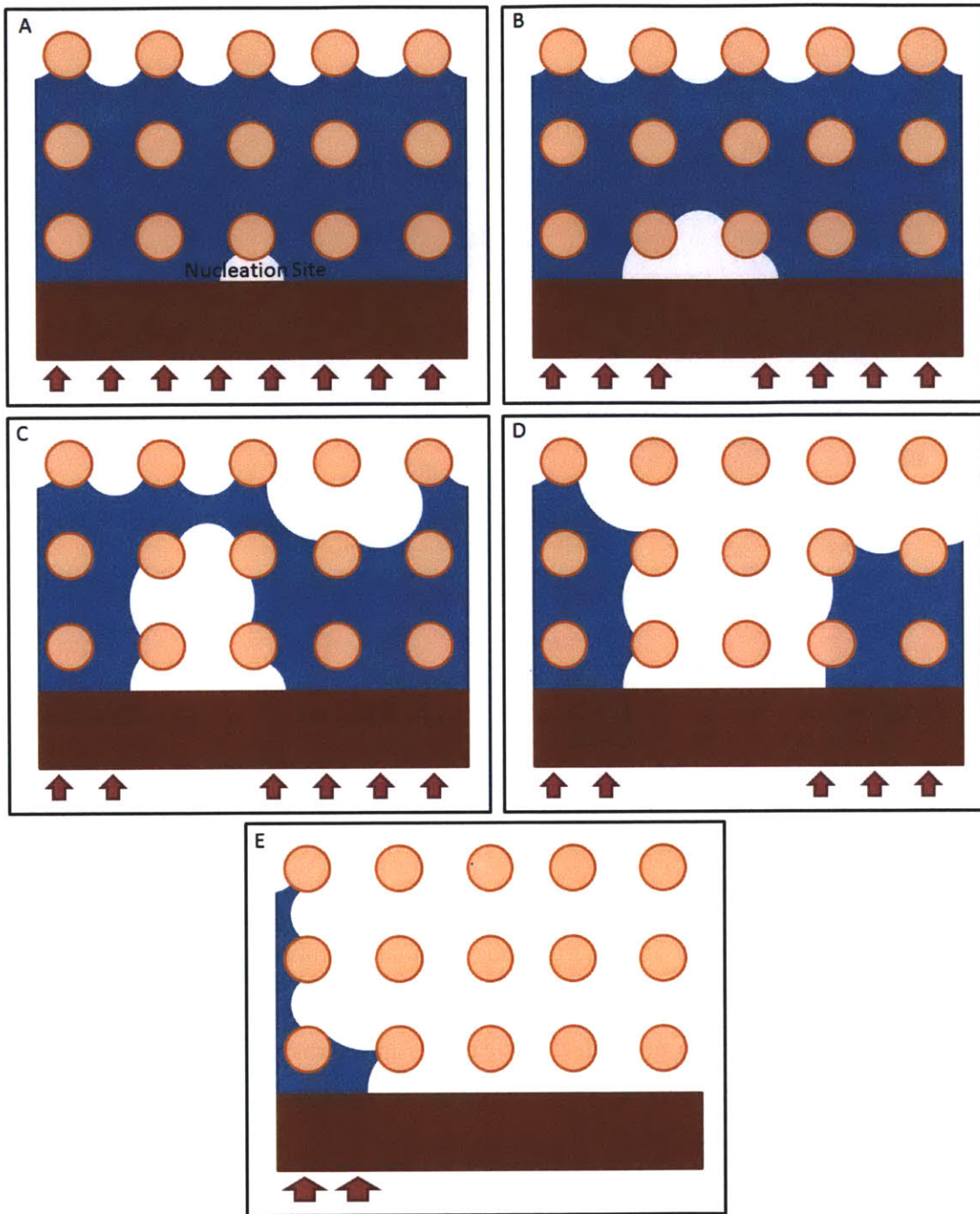
Figure 1.3: Stages of heat pipe dry-out. A. The temperature within the wick exceeds the maximum sustainable superheat within the wick and a vapor bubble nucleates. B. The elevated temperature is sustained and the bubble grows. C. As the bubble grows it chokes the liquid supply and downstream the liquid level begins to fall. D. When the bubble grows large enough to intersect the capillary meniscus the downstream liquid supply is cut off completely. Also, in the absence of liquid there is no evaporation so the solid wall temperature increases and the heat flux decreases at the dry areas. E. The wick completely dries out downstream of the nucleation site.

Fortunately, the effective cavity size of the wicks used in heat pipes is on the order of 5-100 μm and often less than the size of the critical radius for nucleation. As such, bubbles are less likely to form, due to the suppression of the capillary pressure of the wick. The thermodynamics of this suppression is understood, but the practical limitations are unknown. The aim of this project is to advance that knowledge.

# 2 Fabrication of Sintered Metal Wicks

A fabrication study was performed on sintering wicks with Arthur Kariya and Professor Evelyn Wang at MIT's Device Research Lab.

Sintered wick porosity, pore size, permeability, and thermal conductivity are functions of the particle size of the metal powder used and the furnace heat and run time. A controlled atmosphere free of oxygen is critical for avoiding oxidation and successful sintering and requires temperatures from 40% to 90% of the melting temperature. To meet these demands a quartz tube furnace was used with a flow of nitrogen gas and a 95% nitrogen / 5% hydrogen gas in a Lindberg-Blue furnace (HTF55667C) with a six inch diameter tube and is pictured in Figure 2.1.
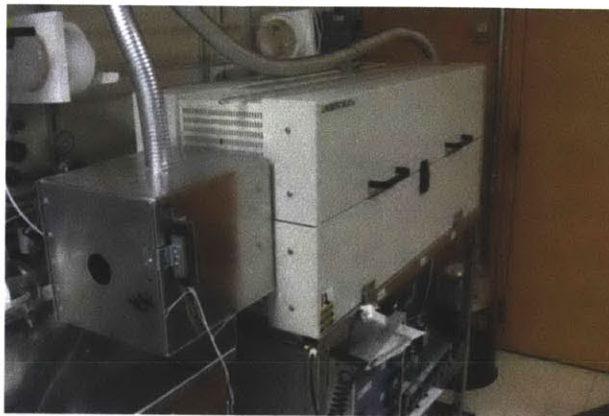


Figure 2.1: Quartz tube furnace for sintering.

Samples must be loaded on a quartz boat and slid into the middle of the tube at the heated section. The boat and a typical sinter batch are pictured below in Figure 2.2.



Figure 2.2: Furnace boat and sinter batch.

Also pictured in Figure 2.2 is the primary method for sintering test samples. The long bar in the middle of the boat is a graphite sheet with a pocket milled out to hold the metal powder. Graphite is an ideal mold because metal will not sinter onto it. Other wicks were made on steel molds but those tended to bond in place.

The wicks were inspected under a scanning electron microscope to gauge the degree of sintering and monitor our control over the process. These images also give as qualitative sense of how water will flow through a wick and what nucleation might be like inside a wick. Figure 2.3 shows a sample selection of wicks.
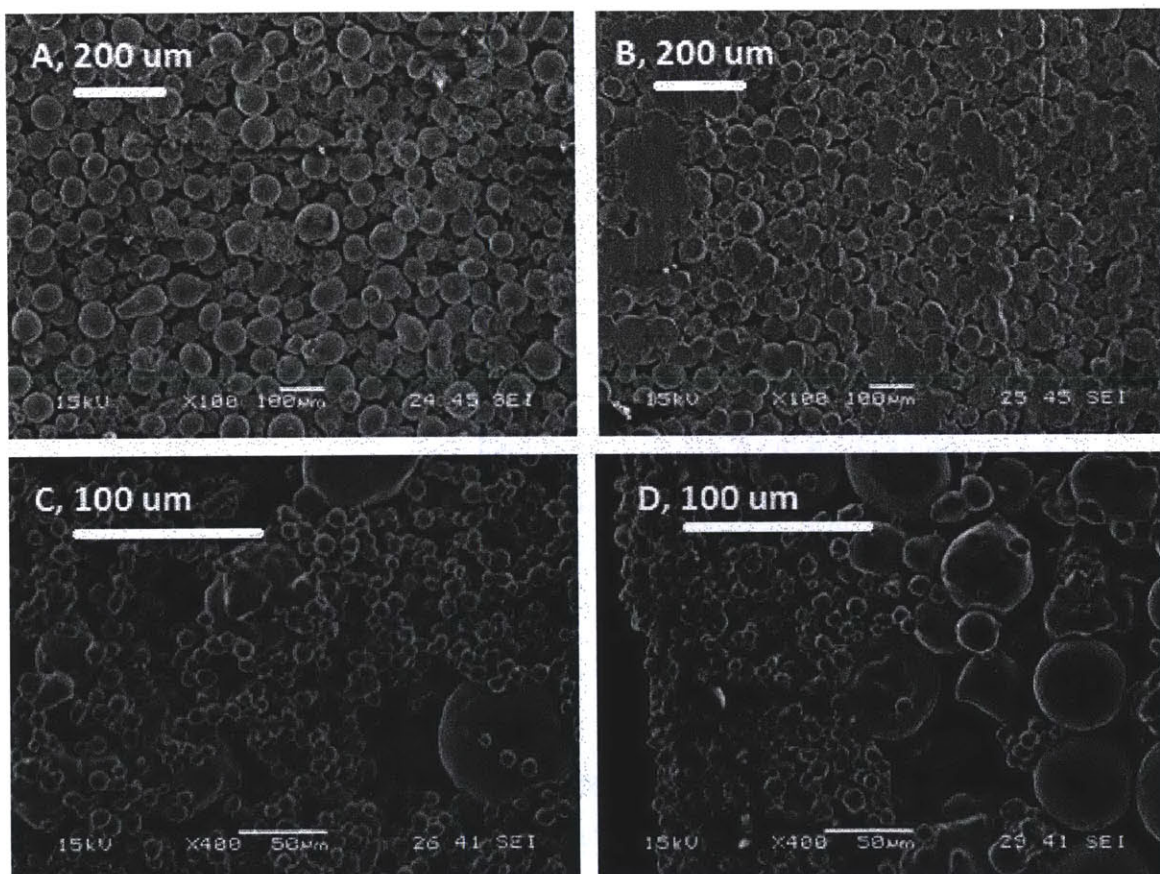


Figure 2.3: SEM images of copper wicks. A: 100 μm powder, B: 100 μm powder after light grinding, C: top view of dual layer wick composed of 10 μm powder on 100 μm powder, D: side view of dual layer wick.

# 3 Description of Proposed Experimental Setup

## 3.1 Design Considerations

Nucleate boiling must be induced in a wick in controllable conditions. The primary challenge and focus of this study is achieving measureable nucleation inside a wick at a known temperature. Since the nucleation should happen inside the wick, visual sensing is not an option for determining when and where the bubble is formed. Thus the wick must be designed such that nucleation does not happen somewhere else in the system and a new method for detecting the moment of nucleation must be determined. As long as there is a sufficient temperature drop across the wick such that the temperature at the surface of the wick is less than the boiling temperature of the free liquid then nucleation should always happen at the hottest part, the inside, of the wick. The following requirements must also be met.

1. Since this experiment will be repeated many times to check data quality and vary wick parameters the device should be easy to load.

2. The wick manufacturing method should be streamlined to expedite the creation of many wicks.

The main components of the physical system are the wick, heater, case, pressure sensor, and pressure compensation tank. These will be complemented by a LabView data acquisition system to monitor the pressure and heat flux.

The wick will be sintered on to a thin baseplate which will clamp onto the case. An O-ring will make the seal watertight and thermally isolate the baseplate from the case. The heater will press against the wick baseplate from below, aligned with the center of the wick. The heater will be an aluminum rod heated by a cartridge heater with three thermocouples inserted at intervals along the axis so that the temperature gradient and thereby heat flux into the device can be determined. Cooling pipes will wind around the top surface of the case and remove heat from the system.

In order to accommodate different saturation temperatures the device will be connected to a two-phase pressure reservoir. The temperature of the reservoir will be controlled so as to govern the pressure inside the wick device.

Figure 3.1 is a system diagram outlining the key components and Figure 3.2 is the simplified model that will be considered by the FEA program when solving temperature profiles.
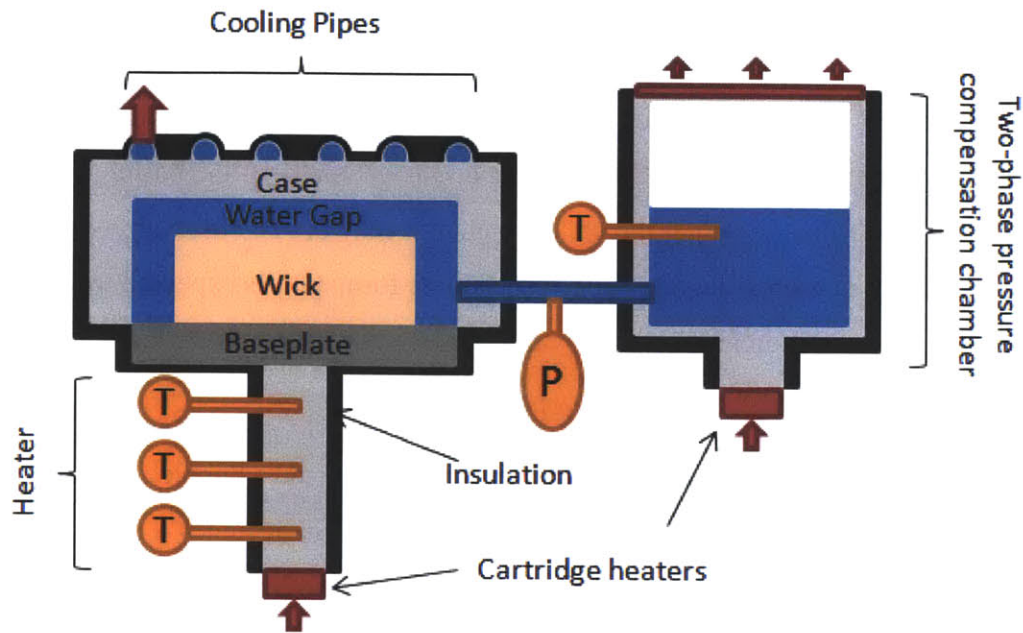
Figure 3.1: Schematic of test device
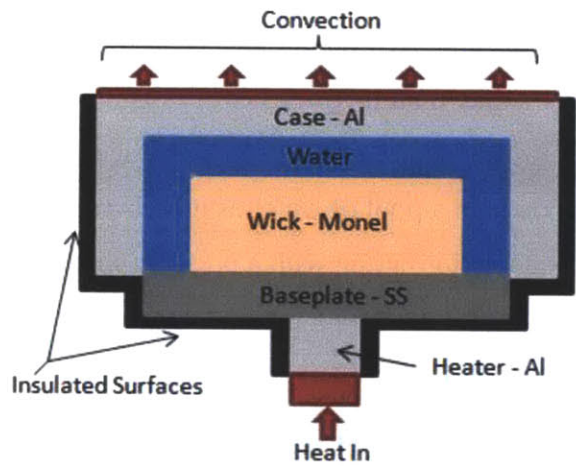


Figure 3.2: Simplified model showing materials and boundary conditions as will be used in thermal modeling. The convective top surface interacts with the ambient temperature through a constant convection coefficient with units of [W/m2K].

# 4 Preliminary Study: Detecting Nucleation

As a first step, the onset of nucleation in an open chamber was observed to evaluate two candidate methods for detecting nucleation: pressure rise from volume expansion and the pressure spike from a bubble overcoming the suppression pressures to achieve the critical radius. The pressure rise from volume expansion depends on the geometry of the boiling vessel. Since the volume of one bubble is so small the pressure change may not be observable over environmental noise. The pressure rise caused by bubble formation is expected to be related to the pressure within small bubbles as given by the Laplace equation

$$D_p = \sigma \left( \frac{1}{r_1} - \frac{1}{r_2} \right) \tag{3.1}$$

Where $D_p$ is the difference between the pressure inside and outside a bubble, $\sigma$ is surface tension, and $r_1$ and $r_2$ are the radii of curvature. For a sphere $r_1 = r_2$ so (3.1) becomes

$$D_p = \frac{2\sigma}{r} \tag{3.2}$$

For water, $\sigma = 0.0728$ N/m, and nucleate bubbles are typically on the order of 10-100 μm so that means the pressure inside nucleate bubbles are on the order of 1000 to 10000 kPa higher than the pressure of the surrounding liquid. A pressure change of that magnitude is easily detectable on common pressure gauges but it was unclear whether the signal would be sustained long enough to move the pressure transducer's diaphram or wheather the signal would be dampened by the body of liquid between the nucleation zone and pressure transducer. To determine this, a rig was built to monitor the pressure change in a pool of water as it boils while looking through a port to visually match the moment of bubble formation with a pressure spike.

## 4.1    Test Rig

A test rig was designed to give visual evidence of nucleation in conjunction with continuous pressure sensing. The test rig was built on the order of the size expected for the final device, 4x4 inches wide and 2 inches tall. The rig consists of an aluminum plate with a 2x2 inch pocket milled out to house the water and serve as the nucleation chamber. A pipe leading to the pressure transducer was soldered onto the side of the device such that it fills with water and listens to the boiling. A thermocouple was inserted into the nucleation chamber body.
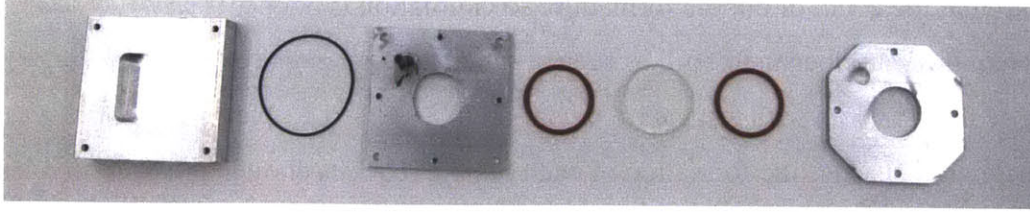
Figure 4.1: Components of test rig.
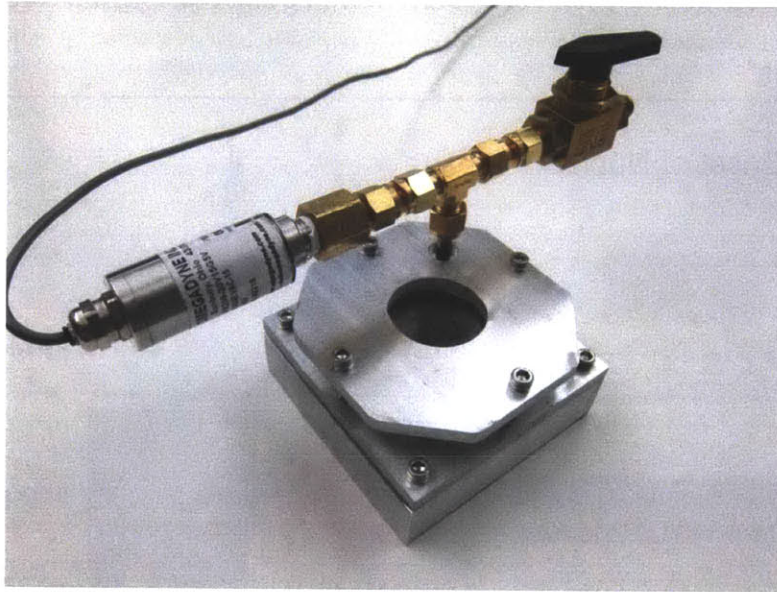


Figure 4.2: Initial test rig assembly.

The pressure sensor used is an Omegadyne PX209-30V15G5V gauge transducer with a range from vacuum to + 15 psi, connected to a National Instruments data acquisition card (USB-6251 and SCB-68) recording 80 samples per second.

## 4.2 Results

After filling the device with water and removing the trapped air such that the pressure sensor was in communication with the heated water the pressure sensor gave a clear indication of nucleation. Tests were run with the fill tube open to atmospheric pressure. While the water was heating up the pressure reading gave a steady average of 104.2 kPa with a standard deviation of 101 Pa. 104 kPa is higher than expected for atmospheric pressure – an indication that the pressure sensor was not properly calibrated – but this study is only interested in the change in

pressure around the event of bubble formation, so calibration is not necessary.

When the water began to boil, as seen at time t=135 s in Figure 4.3, the average pressure reading rose to 104.9 kPa with a standard deviation of 378 Pa. The average pressure was higher during nucleation because the formation of each bubble requires enough pressure to overcome the compressive force of surface tension. The high standard deviation is due to the momentary nature of the pressure spikes. The average pressure value increased because there were many bubbles being nucleated at once. Although visual indication was not possible due to the fogging of the viewport, a clear hissing sound of bubbles forming and bursting indicated boiling.
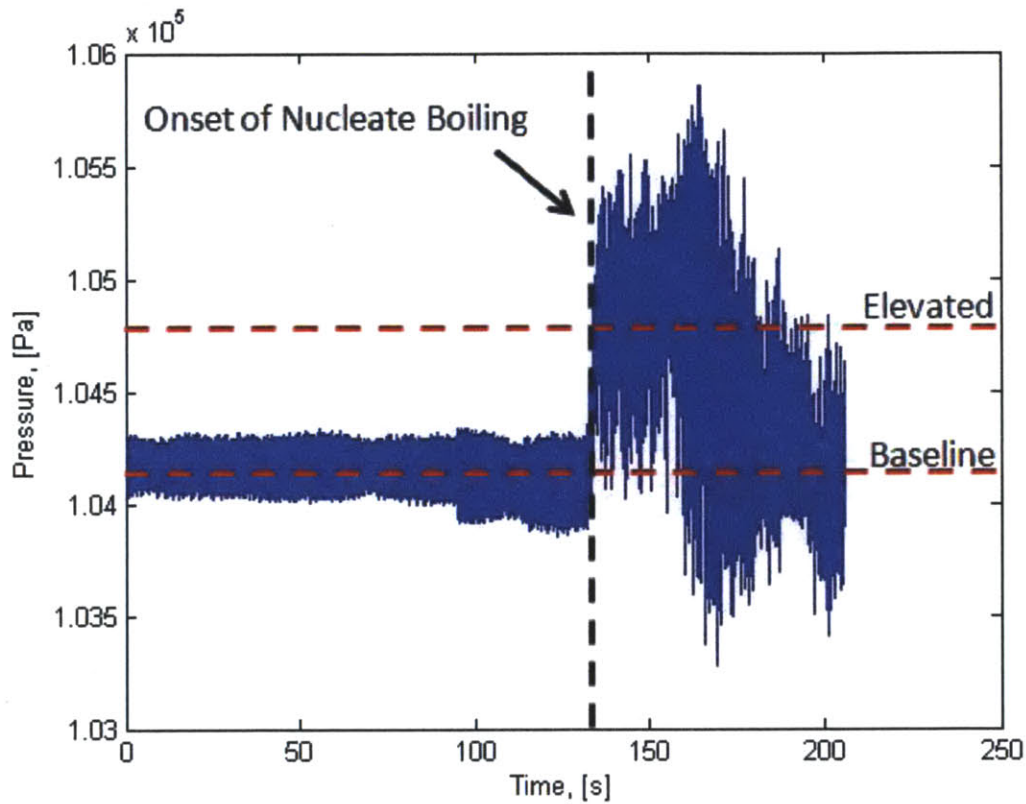


Figure 4.3: Pressure sensor output, nucleation begins at t=135 s where pressure jumps from the baseline reading to an elevated level.

To confirm that the pressure signal would register through small amounts of water this test was repeated with a very thin layer of water and heated with a torch. The water started boiling very quickly and registering the high pressure value. The rig was then tilted so that the boiling water was out of contact with the pressure sensor pipe and the pressure fell back to the atmospheric level. The "tilt device" callout in Figure 4.4 shows the pressure response when the

pressure sensor is tilted first out of contact with the boiling water then back into contact. As shown in Figure 4.4 below, the response time of the pressure sensor to this "tilt-induced onset of nucleate boiling" was nearly immediate, as pressure jumps between high and low in seconds. This suggests that the pressure sensor is sensitive to pressure signals communicated by a very thin layer of water and that it will be responsive in the wick device as well.
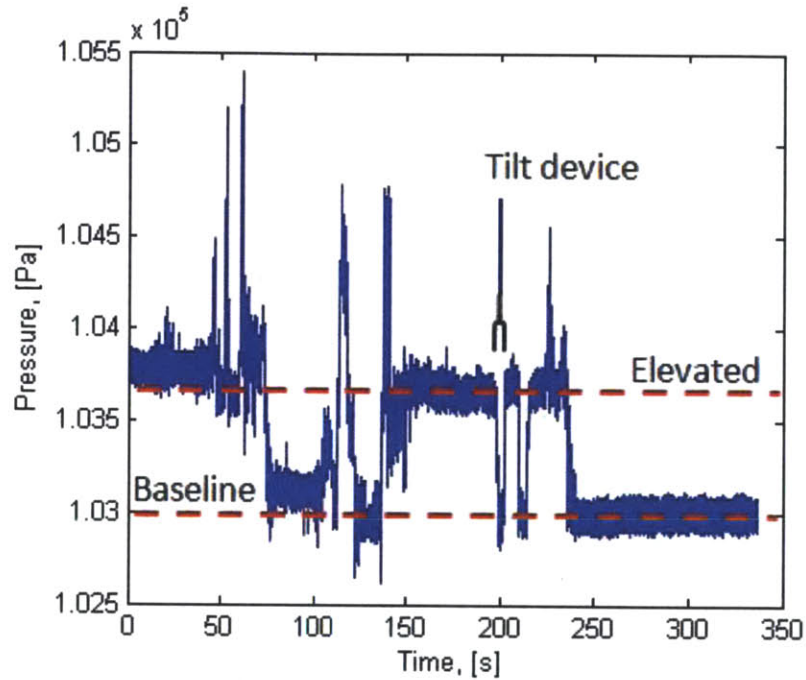


*Figure 4.4: Nucleate boiling pressure signal response time is on the order of seconds. The pressure transducer was tilted in and out of contact with the boiling water at a rate of one cycle per ten seconds at t=200 s. In this time the pressure sensor detected the correct pressure.*

# 5  Design of the Nucleation Test Rig - Thermal Model

## 5.1  Description of Objective

For a proper experiment, the device must be designed to ensure that the point most favorable for nucleation is within the wick, and boiling on the wick surface must be prevented. Thus, the temperature at the center of the wick must be greater than the temperature required for nucleation within the porous material but the temperature at the edge of the wick must be less than the normal boiling point of water at the pressure of the device. It is therefore crucial to design the experiment with the correct thermal attributes. A thermal model of the device was constructed such that it would allow for the design of an effective device and also serve to inform the operator of the temperature profile of the wick during experimentation.

The device design objectives are:

1. Achieve a temperature drop across the wick greater than the porous nucleation superheat.
2. Maintain the surface of the wick to be near to or below the boiling point.
3. Function with wicks of various conductivities.
4. Function at a range of nucleation temperatures.
5. Minimize material consumption.
6. Minimize heat input.

## 5.2  Key Model Elements

The primary goal is to maintain a temperature drop across the wick that is large enough to induce boiling within the wick but not at its perimeter or anywhere else in the device. The simplest geometry which achieves this while minimizing the material used is a sphere, or hemisphere heated at the center, and cooled at the perimeter. Spherical geometry is difficult to manufacture and heat, and furthermore, boundary conditions are difficult to define. A cylindrical wick was chosen instead.

The wick will be a cylinder sintered onto a thin base plate. A small diameter heated rod in thermal contact with the heats the wick. The heat spreads a small amount as it passes through the base plate. The base plate is thin to ensure that the temperature gradient is in the radial direction.

The heat enters the wick from below, and diffuses to escape radially and axially to the water gap. The water gap is considered for the model as a dimensional tolerance between the wick and the casing. The water is in contact with the solid metal case which is cooled through the top of the case by the heat exchanger. The device is insulated on its bottom and sides so they are taken as adiabatic. Figure 5.1 below shows the expected thermal gradient within the device.
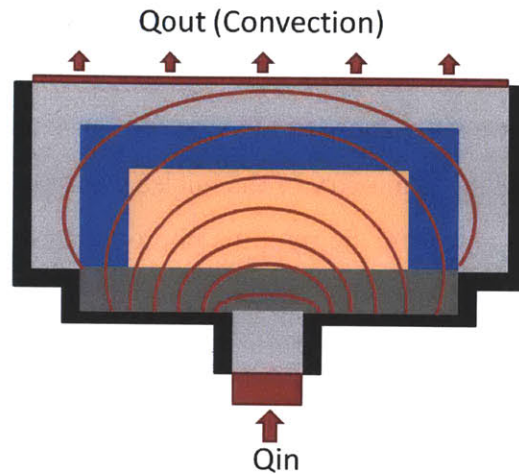


Figure 5.1: Expected thermal gradient within device as shown at a cross-sectional cut about the axis.

Heat flow through the heater and base plate and from the water to the case can be modeled as resistors in series in a rough approximation. A first pass resistor model of the device is shown below in Figure 5.2
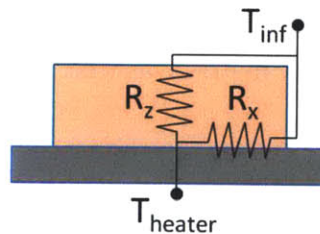


Figure 5.2: Conceptual resistor model of wick. There are no analytical expressions for the effective axial and radial resistances, Rz and Rx, so numeric methods were used to calculate the temperature drop across the wick.

## 5.3 Finite Difference Model

To get accurate temperature predictions for this geometry, a custom finite difference program was made to quickly and easily alter the geometries. Two models were made. The first form of the script uses rectangular coordinates. Rectangular coordinate finite difference analysis, (FDA), implementation is the most versatile form – it can give quick results for any geometry as long as the mesh size is sufficiently fine. Early in the design process it was desirable to have a tool which could operate on any geometry. A drawback of fine meshes can be prohibitively taxing on computational power. The modeling of this device ultimately required too fine a mesh for reasonable desktop computing. To improve FDA performance the node structure was simplified to take advantage of the symmetry of the nucleate device. The rectangular script was converted to cylindrical coordinates and the run time improved by orders of magnitude without loss of accuracy. Both the rectangular and the cylindrical implementations function in the following steps:

1. Define physical geometry and boundary conditions.
2. Establish nodal network
3. Derive energy balance for each possible node interaction.
4. Detect neighboring nodes and assign node conditions.
5. Assemble and solve the finite difference equations.


### 5.3.1 Geometric and Property Matrix

The first step in making the finite difference program was to define the physical system in a form that could easily be scaled and manipulated by the user and easily interpreted by the computer. A three-dimensional property matrix was first used for the finite difference analysis in MATLAB.

Each FDA coordinate system allowed for certain exploitation of the device's symmetry. Since the device geometry and boundary conditions are axially symmetric heat will only flow axially and radially. The rectangular FDA computations were reduced by dividing the device into four symmetric quadrants. The cuts were set as adiabatic and aligned with the mesh. The device was divided into uniform cubes and assigned an index number referencing the material or boundary condition best represented by that node as pictured below in Figure 5.3. The

24

cylindrical FDA was composed of hoop shaped nodes with uniform heights and radial thicknesses. This node structure reduced the unique node count by an order of magnitude and allowed a two dimensional (z,r) representation instead of the three dimensional (x,y,z) representation of the rectangular FDA. The drawback of the radial coordinate system FDA is the limitation to axially symmetric geometries. The key components of the device are radially symmetric and a cylindrical coordinate system defines them well.

The fundamental geometry of the device is simple enough that the material properties can be described by a series of horizontal cross sections (layers): the first layer contains only the heat flux and adiabatic boundary conditions, the second layer contains only the heater cross-section and the adiabatic boundary condition, etc. The rectangular FDA required a two dimensional matrix for each layer because it required three dimensions to capture the geometry of the device. The cylindrical FDA only required a single descriptive dimension per layer so the first row from each of the different layers in the matrix describing the rectangular coordinate system was taken for use in the cylindrical FDA. An example layer which describes part of the axial midsection of the device is shown in Figure 5.3 below.
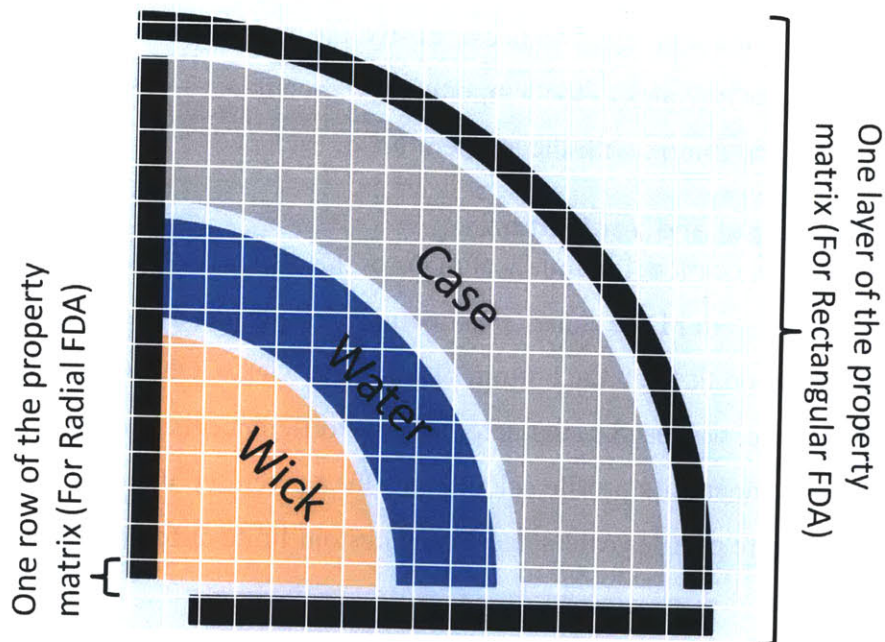


Figure 5.3: One of the nine layers describing the property matrix. Moving radially outward from the center, this layer contains elements of the wick, water, and case surrounded by adiabatic boundary conditions. The script digitizes this geometry by

*choosing which material best represents each node. The rectangular FDA program uses this whole layer to assemble its three dimensional property matrix but the radial FDA program only needs a single row to assemble its two dimensional property matrix.*

Each layer is described by adding and subtracting common matrix regions. Circular areas were discretized to the nearest node point by an automated script called circler.m (see appendix B). Each important feature such as wick radius and wick height was left in variable form. When later optimizing the system I could easily resize features by inputting my desired dimensions and the mesh size. The script then rounded each geometry to the nearest node point and added or subtracted node points and layers as needed.

### 5.3.2         Node Characterization and Finite Difference Matrix

Having established a representation of the physical system, the script needed to identify the condition of each node, (*i.e.* whether internal interacting with like materials, on the surface involved with convective heat transfer). The script indexes each node in the property matrix, then scans through and records the neighboring nodal indices. After matching the neighboring nodes' indices with their property values the script applies the appropriate pre-calculated energy balance (please see appendix A for the energy balances). Lastly, the energy balance is entered into the finite difference matrix as it relates to the temperature of each node. The script solves this matrix and populates the physical matrix with the temperature of each node.

### 5.3.3         FDA Output and Verification

The finite difference model output heat maps of the device. Both the rectangular and the cylindrical coordinate system FDAs show cross sections through the axis and the rectangular FDA shows a cross section through the bottom plane of the wick. COMSOL, a commercial finite element analysis package, was used to validate the finite difference models. Figure 5.4 below shows the COMSOL temperature profile calculations for a given set of parameters while Figure 5.5 shows the temperature profiles calculated by the custom finite difference programs.
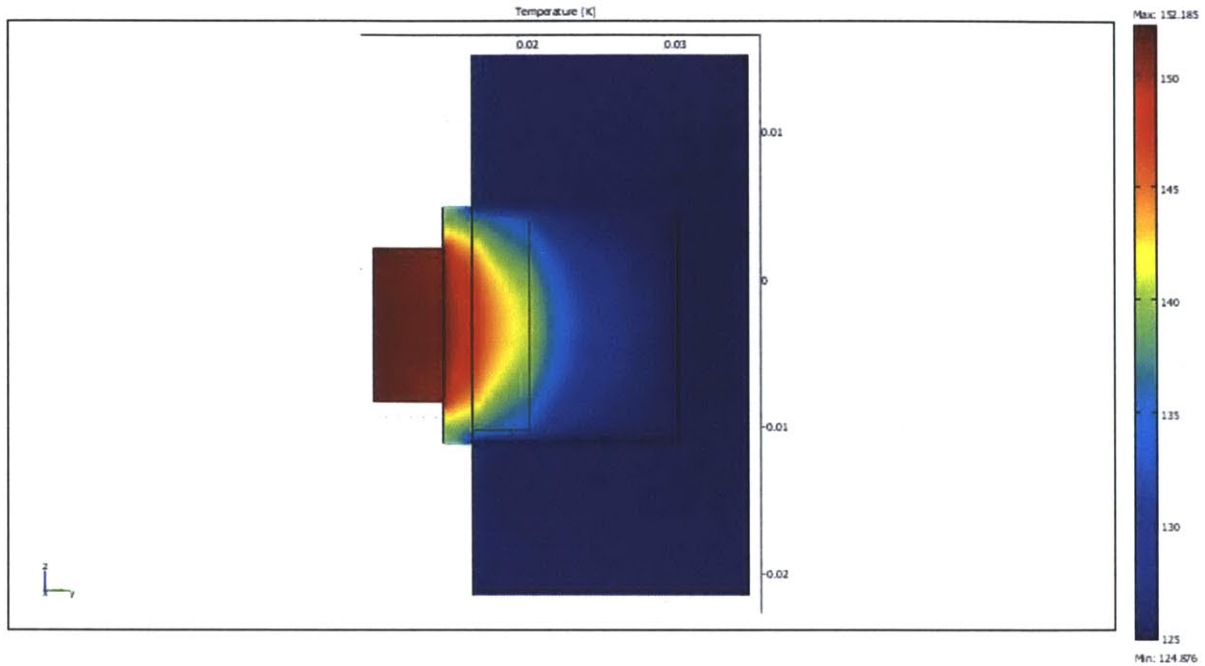
*Figure 5.4: Temperature distribution within wick for given set of parameters according to COMSOL FEA package. The temperature ranges from 124 to 152 ˚C.*



A             B             C
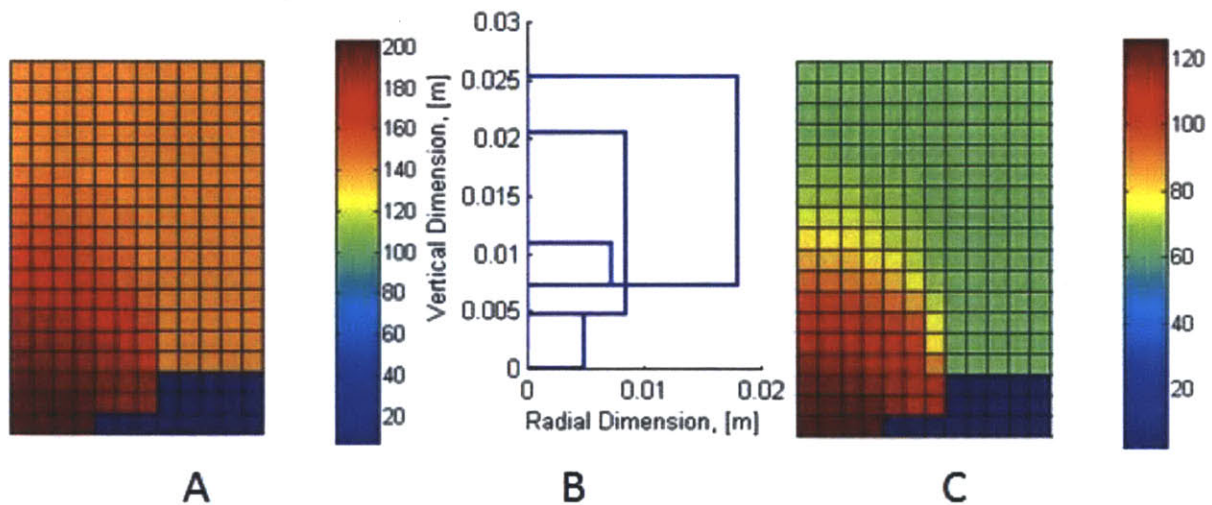
*Figure 5.5: Temperature distributions in the wick with same parameters as modeled in COMSOL in Figure 5.4. Plot (A) is the result given by the rectangular FDA and plot (C) is the result given by the cylindrical FDA. Figure (B) gives the axial and radial dimensions of the device.*

A temperature drop of about 10 °C and a maximum wick temperature of about 148 °C are predicted by COMSOL. The rectangular FDA calculates a temperature drop across the wick of 8 °C and a maximum temperature of 194 °C. The cylindrical FDA calculates a temperature drop of 8.2 °C and a maximum temperature of 116 °C. The FDA models are able to reliably calculate temperature drop across the wick but the rectangular coordinate version over estimates the overall temperature and the radial coordinate version underestimates the overall temperature. The bugs or else fundamental flaws which caused these discrepancies were not isolated. Future work will seek to correct these errors. The present belief is that the nodal interactions are wrongly defined, or else the element-centric nodal structure introduces errors that are corrected by the more traditional element-corner nodal structure. See Appendices A and B for details on the nodal interactions.
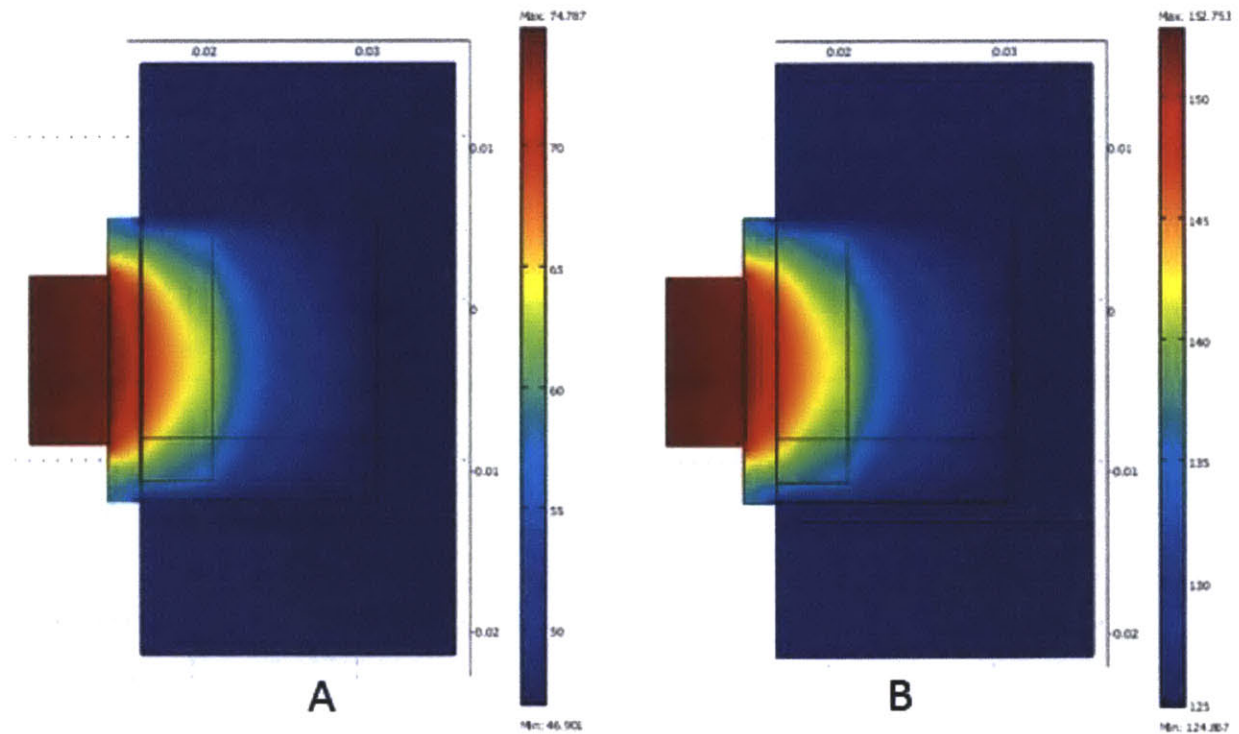


*Figure 5.6: Similar wick geometry as was studied in these figures. Plot A has a convective heat transfer coefficient of 100 W/m²K while plot B has the same convective coefficient as the previous models at 37 W/m²K. Plot A ranges from 46 to 75 °C and plot B ranges from 125 to 152 °C.*

As is shown in Figure 5.6, adjusting the boundary conditions brings the maximum wick temperature down past the level seen in the rectangular FDA model of Figure 5.5 A. The temperature drop does not change. Thus, although the FDA models do not describe the real system with complete accuracy, they do give reliable temperature drop calculations and a suggestion of the temperature profile. The primary difference between the FDA models and COMSOL method is that they keep a fixed mesh size. Small features are given no more attention than large continuous regions thus a lot of computational power is wasted. The FDA models provide rapid insight into the influences of system parameters and are used to specify the non-wick dimensions. As the wick is the most critical component of the system COMSOL was used to finalize the wick dimensions.

# 6 Device Optimization

## 6.1 Design Goals

The device should be able to sustain a temperature drop across the wick greater than the superheat need to cause nucleate boiling at a given pressure so that the water outside the wick does not boil. The target temperature drop is 30 °C. This way, a superheat of 30 °C can be established in the hot zone of the wick while the surface of the wick may remain at saturation. The target maximum temperature in the water outside of the wick is 40 °C.

## 6.2 Analysis Procedure

There are multiple parameters that will influence the performance of the device. The first step in optimizing the device was to identify each of these parameters and assign a range of appropriate values. For each of these parameters a nominal value within the specified range was chosen as a baseline. After setting the baseline, each parameter, beginning with those on the periphery which have the least complicated influence on the total system, was adjusted within its acceptable range and its influence on the temperature drop and maximum free liquid temperature were assessed. Throughout the testing process the overall heat transfer coefficient, UA, and the total heat input to the system were held constant so the areas over which these boundary conditions act could change and alter the flux without altering the net property value. The dimensions considered are shown in Figure 6.1 below.
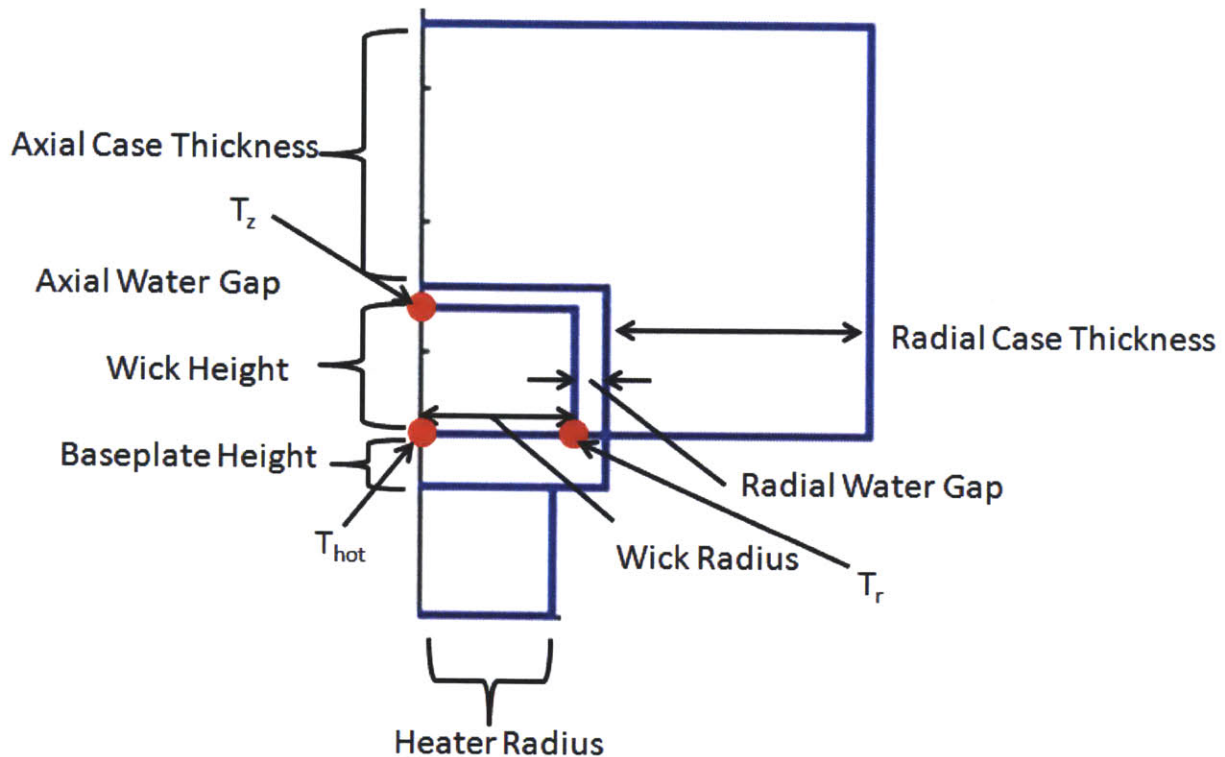
*Figure 6.1: Key wick dimensions shown on one half of the axial cross section of the device.*

## 6.3 Device Features

### 6.3.1 Case

The thickness of the casing which contains the water is one of the most flexible parameters. The requirements for the case are that it is structurally sound enough to prevent water leakage at pressures ranging from zero to two atmospheres and that it minimizes thermal resistance between the heated wick and the cooling surface. Aluminum is quickly apparent as the best material for the case. It is strong, highly thermally conductive, easy to machine, and inexpensive.

Any thickness greater than about 1 cm will be strong enough to support the pressure range (0.5 atm vacuum to 0.5 positive pressure). Anything smaller would be impractical for clamping. The design of the case will then be controlled by thermal resistance considerations.

The starting point for the case thickness optimization is 1 cm. Thickness will be varied until increasing thickness no longer lowers the maximum temperature in the wick.

### 6.3.2 Baseplate

As the baseplate is mounted to the wick and a large temperature drop across the wick is required the baseplate must have a high resistance to radial heat flow. Also, the baseplate must be strong enough to support the device's operational pressure range. Stainless steel is a good material choice because it has a low thermal conductivity and high strength.

The baseplate radius is coupled with the water thickness since the baseplate is responsible for containing the water in the device. Thus the radius of the baseplate will not be considered as one of the independent design parameters. Its influence will be expressed with the variation of the radial thickness of the water. The thickness of the baseplate is, however, a key parameter. Reducing the thickness of the baseplate increases the radial resistance and decreases the axial resistance to both improve the temperature drop and reduce the amount of heat needed to cause nucleation.

Stainless steel sheet metal is readily available in 1 mm increments for thicknesses below 1 cm. The baseplate thickness was set at 2 mm. If, during construction, it is found that 2 mm is needlessly large or too small it can be adjusted.

### 6.3.3 Heater

The heater should not be a source of thermal resistance so a conductive material like copper or aluminum is used. The smaller the radius of the heater, the more concentrated the hot spot will be, and the thinner the wick radius can be. However, the heater should not be too narrow; holes must be drilled in the heater for thermocouple mounting. Also, if the hot zone is too narrow, then the size of the nucleation zone may be too small to give a strong reading on the pressure sensor.

A baseline heater radius was set to 5 mm. This value would only be altered if adjusting the other parameters would not do enough to achieve the specified device goals.

32

### 6.3.4  Wick

Kariya and Dominguez-Espinosa used the laser flash method to measure the conductivity of porous metals during his research in sintered wicks [3]. Dry-wick conductivity values of 1 to 2 $W/m^2K$ for sintered stainless steel, about 2 $W/m^2K$ for sintered monel, and about 100 $W/m^2K$ for sintered copper are reported. Although the laser flash method cannot be used to measure the conductivities of wet wicks the conductivity of a wet sintered wick should be somewhat better than that of a porous sintered wick because the air cavities are be replaced by water. However, water has such a low conductivity and the porosity of sintered wicks of spherical powder is typically about 50% so the conductivity of a wet wick should not be substantially higher than that of a dry wick.

The radial and axial dimensions of the wick are the most critical dimensions in the model as they determine the gradient in the wick. The hottest points on the outside surface of the wick are those nearest the hot center: the center point of the top face and the circle where the side walls meet the baseplate. Boiling at either of these places is equally undesirable, there is no advantage to having one hot spot cooler than the other. The extra material that goes into increasing the resistance of one dimension beyond the resistance of the other dimension is wasted because the temperature drop across the wick is only as good as the lowest resistance. To minimize material consumption and simplify the design, the radial and axial temperature drops were set equal to each other.

The wick size is limited as the metal powder used to make these wicks is expensive, and the furnaces available cannot take samples larger than 6 inches in diameter. Furthermore, as wicks get larger the sintering process becomes less reliable. The wick radius and height baseline dimensions were set to 6 mm and 5 mm respectively, and varied with the intention of minimizing volume and maximizing temperature drop. The baseline thermal conductivity was set to 4 W/mK.

## 6.4   Summary of Baseline Feature Parameters

Table 6.1: Baseline input parameters

|  | Heater | BasePlate | Wick | Case |
|---|---|---|---|---|
| Radial Dimension, [mm] | 5.2 | Dependent | 6 | 10 |
| Axial Dimension, [mm] | Arbitrary | 2 | 4.8 | 10 |

| Qin, [W] | UA, [W/K] | Tinf, [C] | Kwick, [W/mK] | Step Size, [mm] |
|---|---|---|---|---|
| 5 | 0.04 | 20 | 4 | 0. 4 |
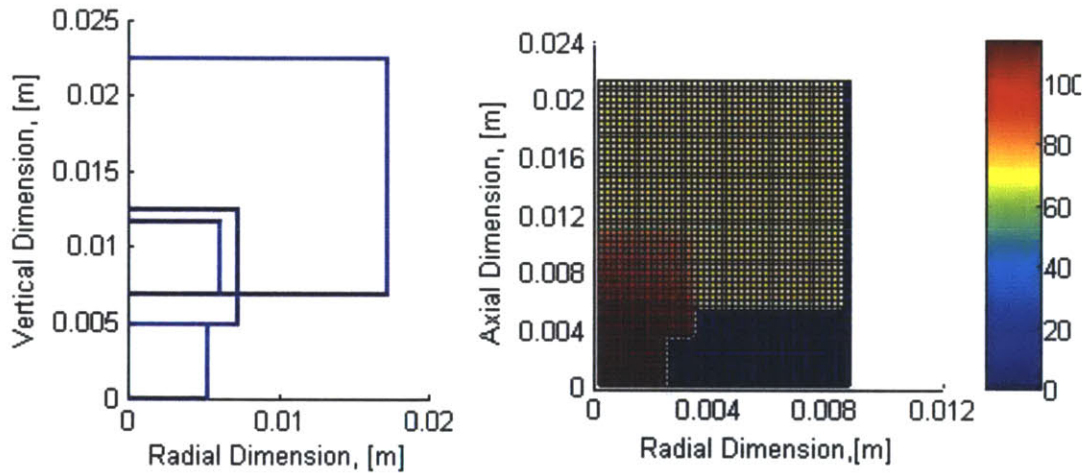


*Figure 6.2: Baseline geometry and temperature distribution*

Table 6.2: Baseline output temperatures.

| $T_{hot}$, [C] | $T_z$ | $T_r$ | $T_{case\ center}$ | $T_{case\ edge}$ | h, [W/m^2K] |
|---|---|---|---|---|---|
| 106.3386 | 86.6798 | 100.112 | 71.6743 | 71.6488 | 43.0381 |

### 6.4.1   Baseline Performance

The baseline parameters show a temperature drop of 20 °C axially and 6 °C radially across the wick. The radius needs to increase from the baseline value to balance the steep axial

34

resistance. The maximum temperature of 106 °C exceeds the design target of 70 °C. The heat map shows the case is much thicker than it needs to be to give a good thermal representation of the device. The temperature at the outer limits of the case is only 0.1 degrees less than that of the inner limits. Reducing the thickness within the thermal model will improve computational speed at little cost of accuracy.

## 6.4.2 Varying Feature Parameters

The wick dimensions affect both the maximum temperature in the wick, $T_{hot}$, and the temperature drop across the wick. All other parameters (ie. case thickness, water gap) only influence $T_{hot}$ thus only $T_{hot}$ was observed during their variations.

The case vertical and radial thicknesses were varied between 1 mm and 15 mm. As the vertical thickness of the case increases $T_{hot}$ increases but only by 0.1 degrees from 5 to 15 mm of thickness. The working value of the vertical case thickness was set to 5 mm. Increasing radial thickness from 1 to 15 mm caused $T_{hot}$ to decrease 0.8 degrees. Increasing radial thickness beyond 1 cm has nearly no effect on $T_{hot}$. The working value for the radial case thickness was left at 1 cm.
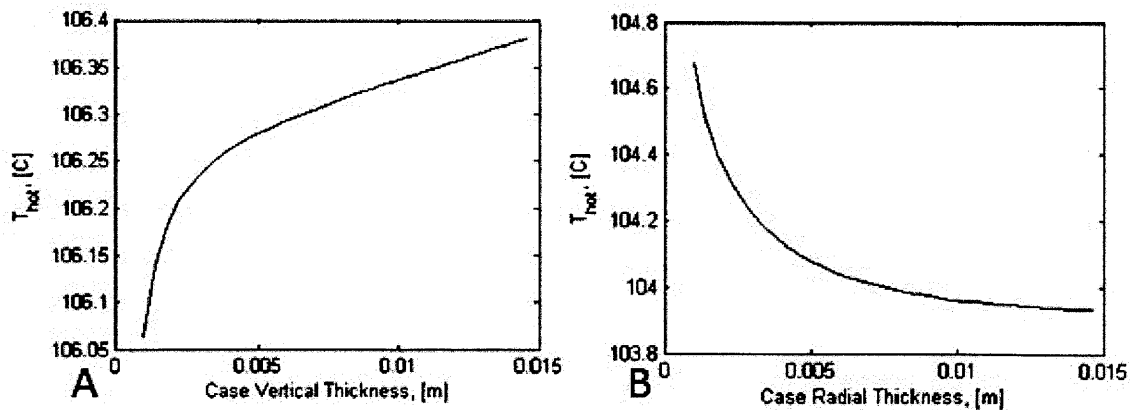


Figure 6.3: Varying the case thickness about its baseline value of 1 cm in the vertical direction (A), and in the radial direction (B).

The baseplate thickness was varied from 0.4 to 14 mm to understand the influence manufacturing defects will have on the system. Above 0.4 mm, increasing baseplate height has

nearly no influence on $T_{hot}$ or the temperature drops across the wick. This is because after that point the heat has nearly evenly diffused along the cross section of the baseplate and its center point is not so preferentially heated. The working value will remain at the baseline 2 mm and manufacturing variation will have little effect on the system thermal properties.
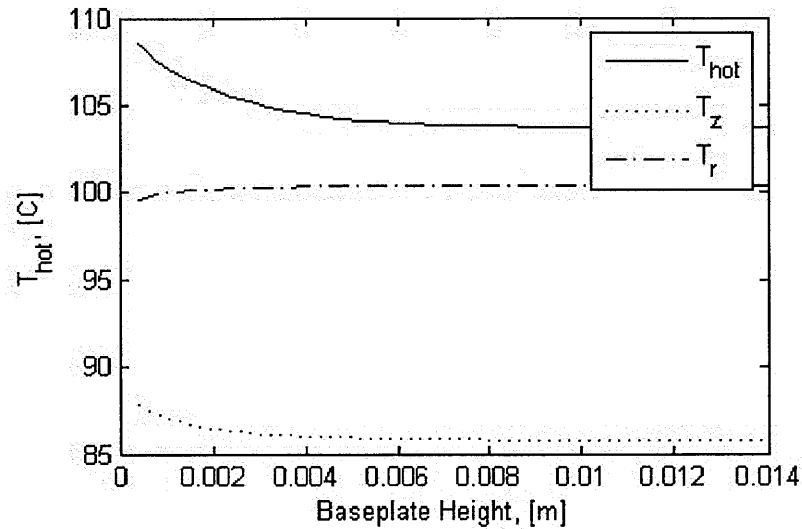


*Figure 6.4: Effect of varying the baseplate height on $T_{hot}$ and temperature drops.*

The heater radius influences the overall model both independently and with its relation to the wick radius. Thus, two tests were conducted; first, the difference between the wick radius and the heater radius was fixed at 0.8 mm; second, the wick radius was fixed at 8.4 mm. In each case the heater radius was varied from 2.4 to 7.6 mm and the heat input was held constant at 5 W.
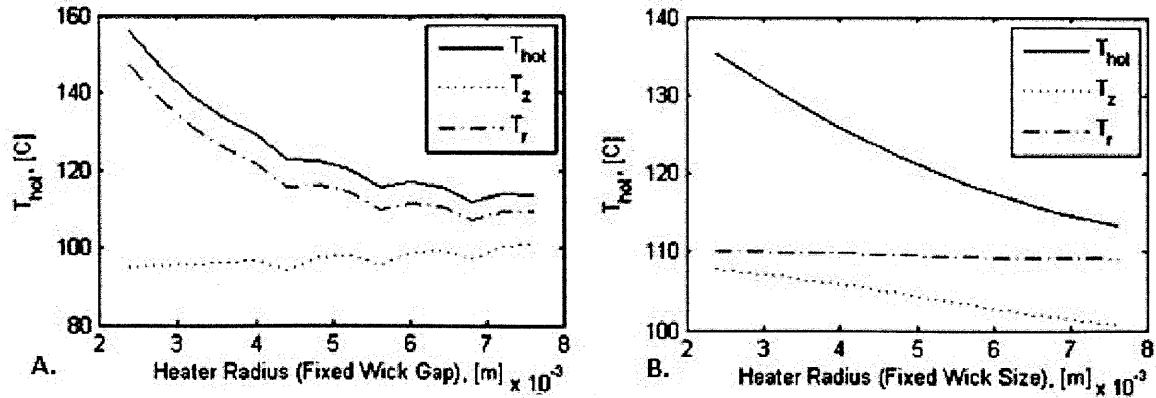
*Figure 6.5: A: Fixed difference between wick and heater radii, B: Fixed wick size. Heater radius varies from baseline value of 5.2 mm and wick radius varies from baseline value of 6 mm.*

During wick optimization the heater radius is held constant. It is helpful to see how the ratio between the wick radius and the heater radius influences the system properties. Plot B of Figure 6.5 is smoother than plot A because generating plot A involved changing the heater and wick radii while generating plot B only involved changing the heater radius. When the FDA program defines it's the material properties of its finite mesh it takes the most represented property of each node and shared nodes are "rounded" off. The more parameters the script has to round off in an iterative loop as in Figure 6.5, the more the associated rounding errors are amplified.

When the wick gap, the difference between the wick and heater radii, was fixed at a constant distance greater than the heater radius, the radial temperature drop across the wick stayed relatively constant as can be seen in plot (a) of the figure above. The length through which the heat flowed stayed the same so the temperature drop should stay about the same. While the heater and wick radii are changing, the temperature on top of the wick stays nearly constant at 99°C. $T_{hot}$ drops, the axial temperature drop decreases due to the decrease in the axial thermal resistance of the wick caused by the increase in area.

When the wick radius is fixed, however, and the heater radius increases, the temperature on top of the wick, $T_z$, decreases while the temperature at the edge of the wick, $T_r$, stays the

same. The temperature on the top of the wick decreases because the heat flux density decreases as the heater area increases.

It is expected that increasing a particular wick dimension, axial or radial, should increase the respective resistance and thereby temperature drop. These two plots show second-level relations between these dimensions and the heater radius. From (a), as the difference between the heater radius and the axial dimension of the wick decreases, $T_{hot}$ decreases, the temperature at the top of the wick stays the same, and the temperature at the radius of the wick decreases. From (b), as the difference between the heater radius and the radial dimension of the wick decreases, $T_{hot}$ decreases, the temperature at the top of the wick decreases, and the temperature at the radius of the wick stays the same.

The working heater radius was kept at the baseline value of 5 mm for the wick testing. Before varying the wick dimensions the baseline values were updated to the new working values as summarized below.

Table 6.3: Summary of working dimensions for wick testing.

|  | Heater | Baseplate | Wick | Case |
| --- | --- | --- | --- | --- |
| Radial Dimension, [m] | 0.0052 | Dependent | 0.006 | 0.01 |
| Axial Dimension, [m] | Arbitrary | 0.002 | 0.0048 | 0.01 |

## 6.5  Wick Modeling

Components outside the wick were kept at the values suggested by the FDA while wick height and radius were varied under a range of heat inputs and wick conductivities. Since changing the wick radius would change the area of the cooled surface the average heat transfer coefficient was scaled from an overall heat transfer coefficient by the area of the cooling surface. The overall heat transfer coefficient was set to an accessible value of 0.14 W/K. The heat input was set at 5 W, a level easily generated and dissipated with bench-top laboratory equipment.

### 6.5.1  Resistance Balance

The first step in optimizing the wick was finding the ratio of wick height to radius which balances the axial and radial temperature drops. This condition is desirable because it minimizes

the wick volume needed to sustain a given temperature drop and is achieved when the temperature at the base edge of the wick equals the temperature of the center of the top surface of the wick, or:

$$T_r = T_z \qquad\qquad (6.1)$$

as shown in Figure 6.1.

To begin, the wick radius, $w_r$, was set 10 mm and the wick height, $w_z$, was varied until the condition in equation (6.1) was met. It was found that a wick height of $w_z=10$ mm balanced the axial and radial temperature drops, and the temperature ratio, $T_{ratio}=T_z/T_r$, is equal to one. Table 6.4 below shows the summary of this process.

Table 6.4: The wick height is varied until $T_{ratio}$ equals one, indicating the optimal wick ratio.

| $W_z$, [mm] | $T_{hot}$, [C] | $T_z$, [C] | $T_r$, [C] | $T_{ratio}$ |
|---|---|---|---|---|
| 4 | 40 | 31 | 27 | 0.692 |
| 6 | 40 | 28.5 | 27 | 0.884 |
| 8 | 40 | 27 | 27 | 1 |

Thus, for a heat input of 5 W, a UA of 0.14 W/K, and a wick radius of 10 mm, the optimal height to radius ratio, $w_{ratio}$*, is 0.8. This gives $T_{hot}=40$ °C and $\Delta T=13$ °C. Both of these values are less than desired. Increasing the heat input or wick dimensions would improve both of these properties because the temperature drop across a resistive element is directly proportional to heat input and length. Having found $w_{ratio}$* for a particular configuration, tests were done to see if this ratio holds for different heat inputs and wick sizes so that wick radius and height could be linked together in further analyses.

### 6.5.2 Heat Input

The heat input was varied from 5 to 15 W while the wick ratio was held at 0.8, UA=0.14 W/K, and $w_z=8$ mm. Table 6.5 below summarizes the results.

Table 6.5: Vary heat input for fixed wick ratio.

| $Q$, [W] | $T_{hot}$, [C] | $T_z$, [C] | $T_r$, [C] | $T_{ratio}$ | $\Delta T$, [C] |
|---|---|---|---|---|---|
| 5 | 40 | 27 | 27 | 1 | 13 |
| 10 | 80 | 54 | 54 | 1 | 26 |
| 15 | 120 | 81 | 81 | 1 | 39 |

The increased heat input does not change $w_{ratio}^*$. This is because the proportion of heat traveling in the axial and radial directions is the same for high and low heat inputs since internal heat flow depends primarily on geometry and material properties. For every heat input the ratio of the axial and radial temperature drop stays the same. This study shows that once $w_{ratio}^*$ is determined for a particular heat inputs it will stay the same for all heat inputs. Further, this study shows that the temperature drop and maximum wick temperature are directly proportional to heat input. For this geometry

$$\Delta T = 2.6Q \qquad\qquad (6.2)$$

$$T_{hot} = 8Q \qquad\qquad (6.3)$$

for $w_{ratio}$=0.8, $w_z$=8 mm, $K_w$=4 W/mK, UA=0.14, and $5W \leq Q \leq 15W$

This result shows that the critical wick temperatures, $T_{hot}$ and $\Delta T$, can easily be tuned by altering the heat input. The constant terms in equations (6.2) and (6.3) will be different for wicks of different sizes. These constant terms represent the effective resistance across the wick and through the device respectively. This can be seen by rearranging the resistance form of the heat transfer equation as

$$\Delta T = RQ \qquad\qquad (6.4)$$

### 6.5.3   Scaling
Increasing the wick size will increase the effective resistances. The most efficient way to increase the wick size is by increasing the wick radius and height together such that the optimal wick ratio is maintained. However, the optimal wick ratio may not be the same for all dimensions: a larger wick may require a different ratio of thickness to radius for equality in the axial and radial thermal resistances. The relation between optimal wick ratio and wick size was studied by increasing the wick height and observing the change in $T_{ratio}$ while $w_{ratio}$ was kept at 0.8. Table 6.6 shows that although the ratio of 0.8 is optimal for a wick with a height of 8 mm, the ratio is likewise applicable for thicker wick sizes, as $T_{ratio}$ deviates a little from one. The results are shown in Table 6.6 below for Q=10 W instead of 5W because increasing heat input makes temperature differences more pronounced without disrupting $w_{ratio}^*$.

Table 6.6: Wick height is varied for fixed wick ratio.

| $w_z$, [mm] | $w_r$, [mm] | $T_{hot}$, [C] | $T_z$, [C] | $T_r$, [C] | $T_{ratio}$ | $\Delta T$, [C] |
|---|---|---|---|---|---|---|
| 8 | 10 | 80 | 54 | 54 | 1 | 26 |
| 9 | 11.25 | 80.75 | 53 | 52.5 | 0.982301 | 27.75 |
| 10 | 12.5 | 81.5 | 52.25 | 51.75 | 0.983193 | 29.25 |
| 11 | 13.75 | 82.5 | 51.75 | 51 | 0.97619 | 30.75 |

As wick size increases the ratio of axial to radial temperature drops decreases at an average rate of 0.8% per mm. Since this difference is so small and the wick height will not be very far from the 8 mm start point the optimal wick ratio can be assumed to be 0.8 mm for all wick sizes.

Increasing the wick height causes a nearly linear increase in the maximum wick temperature and wick temperature drop over the range of wick heights studied. Fitting functions to the relation between wick height and both maximum wick temperature and temperature drop yields

$$T_{hot} = 0.82w_z + 73.4 \tag{6.5}$$

$$\Delta T = 1.58w_z + 13.5 \tag{6.6}$$

for Q=10 W, $w_{ratio}$=0.8, $K_w$=4 W/mK, UA=0.14 W/K, and 8≤$w_z$≤11 mm

These expressions for temperature in terms of wick height are linear for the range of wick heights studied. The true function of $\Delta T(w_z)$ must equal zero at $w_z$=0 because the temperature drop across the wick should become very small when the wick becomes very small. Likewise, the true function of $T_{hot}(w_z)$ should approach something less than the constant term in equation (6.5). However, for the range of $w_z$ which give $\Delta T$ values in the desired range the functions for $T_{hot}$ and $\Delta T$ are well approximated as linear.

Equations (6.2) and (6.6) combine to give $\Delta T(Q,w_z)$ and equations (6.3) and (6.5) - combine to give $T_{hot}(Q,w_z)$.

$$T_{hot}(Q, wz) = \frac{Q}{10}(0.82w_z + 73.4) \tag{6.7}$$

$$\Delta T(Q, wz) = \frac{Q}{10}(1.58w_z + 13.5) \tag{6.8}$$

41

for $w_{ratio}$=0.8, $K_w$=4 W/mK, UA=0.14 W/K, 5W≤Q≤15W, and 8≤$w_z$≤11 mm

Plotting these equations over their specified range of Q and $w_z$ gives
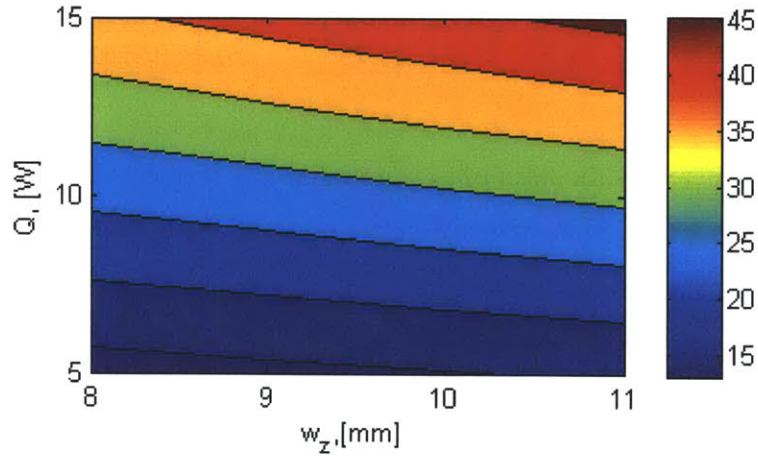


*Figure 6.6: ΔT for Q and linear range of $w_z$.*
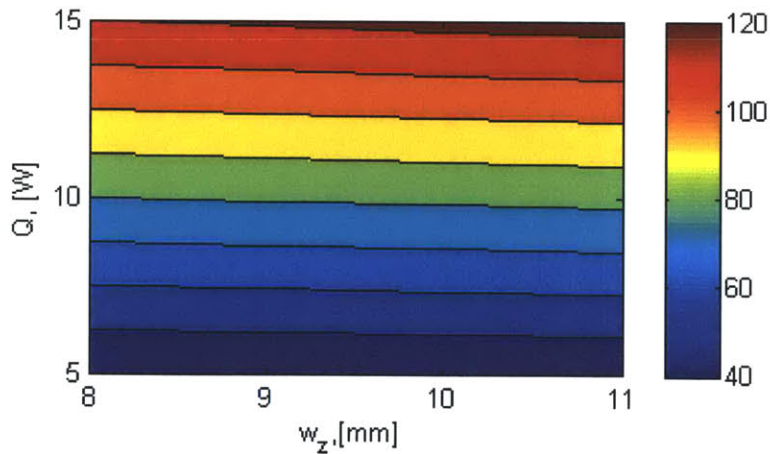


*Figure 6.7: Thot for Q and linear range of wz.*

Figures 6.6 and 6.7 show that Q has a much greater influence on temperature than $w_z$ within the ranges considered. From Figure 6.6 it can be seen that Q≥12 W for low $w_z$ and Q≥10 W for high $w_z$ meet the ΔT specification of 30 °C. $T_{hot}$ is nearly dependent on Q alone. The 70 °C target is only reached when 8≤Q≤10 W. Thus, the parameters represented by these figures do not

meet the combined specifications for $T_{hot}$ and $\Delta T$. As a potential means of reconciling this conflict the UA was then investigated.

### 6.5.4 Cooling

Increasing the UA increases the cooling, which lowers the temperature of the whole system at once. The temperature drop across the system should remain the same. Thus, increasing the UA should serve as a means of bringing $T_{hot}$ down to the target range for the Q necessary to achieve the target $\Delta T$. Simulations were run to observe the effect of UA on $T_{hot}$ and $\Delta T$ for different wick sizes. It was found that $\Delta T$ did not change with UA. The effect of UA on $T_{hot}$ is summarized below in table 6.8.

Table 6.8: Effect of UA on $T_{hot}$ for different $w_z$ with wick dimensions held at the optimal ratio and Kw=4 W/mK.

|           | 8 mm | 9 mm  | 10 mm | 11 mm |
|-----------|------|-------|-------|-------|
| 0.14 W/K  | 80   | 80.75 | 81.5  | 81.5  |
| 0.175 W/K | 70.5 | 71.75 | 72    | 73.25 |
| 0.21 W/K  | 65   | 65.75 | 66.5  | 67    |

From Table 6.8 it can be seen that $T_{hot}$ decreases approximately exponentially as UA increases. The effect is unrelated to wick size as it does not change with $w_z$. Changing the UA has a strong effect on $T_{hot}$. The figure below shows this.
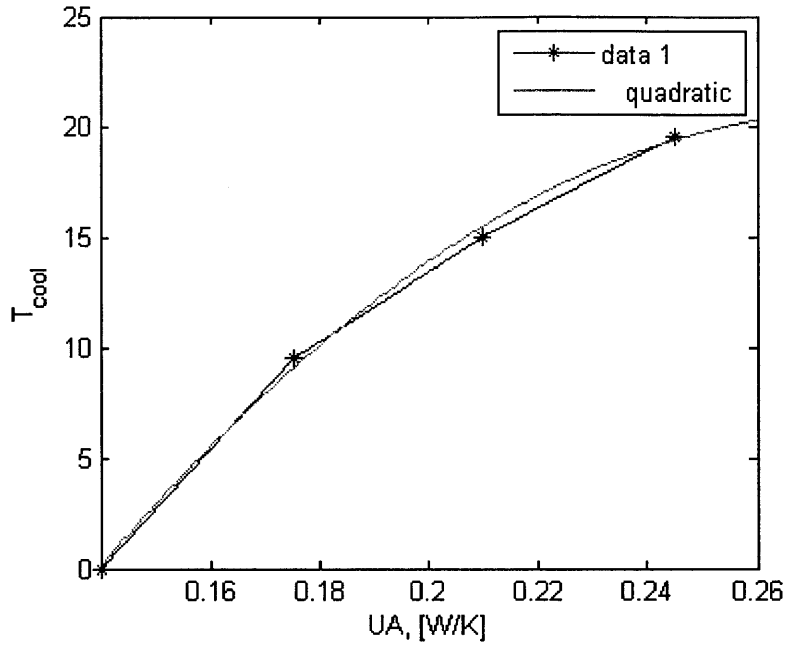
*Figure 6.8: The cooling effect UA has from the baseline UA value of 0.14 W/K on $T_{hot}$.*

From the baseline UA=0.14 W/K, the $T_{hot}$ temperature drop from $T_{hot}$(UA=0.14) is given by the quadradic fit

$$T_{cool} = -1020.4(UA)^2 + 575.71UA - 60.45 \qquad (6.9)$$

which holds for $w_{ratio}$=0.8, $K_w$=4 W/mK, UA=0.14 W/K, 5W≤Q≤15W, and 8≤$w_z$≤11 mm.

### 6.5.5 Conductivity

Finally, the conductivity of the wick was tested for influence on the critical temperatures.

Table 6.9: Effect of wick conductivity on critical temperatures. Q=10 W, $w_{ratio}$=0.8 UA=0.14 W/K,$w_z$=8 mm.

| K, [W/mK] | $T_{hot}$, [C] | $\Delta T$, [C] |
|---|---|---|
| 4 | 80 | 26 |
| 3 | 82.75 | 29.25 |
| 2 | 87.75 | 35.5 |

$T_{hot}$ and $\Delta T$ both increase as $K_w$ decreases. This is expected because decreasing conductivity increases resistance. For the conditions studied in Table 6.9, changing the conductivity had a somewhat exponential effect on the temperatures. The effect is felt more by $\Delta T$ than $T_{hot}$. The wick will be designed to function with $K_w$=4 W/mK. Table 6.9 confirms that any test wick with conductivity less than the design conductivity will still achieve or exceed the desired temperature drop.

# 7 Conclusion

In this study of the design of a device to discern the maximum superheat sustainable by a porous material, a method for detecting bubble formation in a porous material was developed. A preliminary study was conducted to confirm a pressure-based indication of the onset of nucleation. The temperature distribution in the device was parameterized. Three dimensional conduction through the wick was simplified to two dimensional flow via cylindrical symmetry. The two dimensional representation supported a custom finite difference model which gave a rapid understanding of the thermal system. For a more precise understanding of the temperature distribution through the wick, a commercial finite element analysis package was utilized. From these simulations, and design constraints, the two dimensional heat flow model condensed into a one dimensional problem.

The governing wick design equations were found to be

$$T_{hot}(Q, wz) = \frac{Q}{10}(0.82w_z + 73.4) \qquad (6.7)$$

$$\Delta T(Q, wz) = \frac{Q}{10}(1.58w_z + 13.5) \qquad (6.8)$$

for $w_{ratio}$=0.8, $K_w$=4 W/mK, UA=0.14 W/K, 5W≤Q≤15W, and 8≤$w_z$≤11 mm. The temperature drop across the wick can be further improved by decreasing the wick conductivity. The maximum temperature in the wick can be controlled by adjusting the overall heat transfer coefficient.

Choosing $w_z$=8 mm and solving for Q with $\Delta T$=30 °C gives Q=11.47 W. With $K_w$=4 W/mK and UA=0.245 W/K, $T_{hot}$=69.5 °C, thus, the design objectives are met. The temperature profile for these parameters is shown below in Figure 7.1.
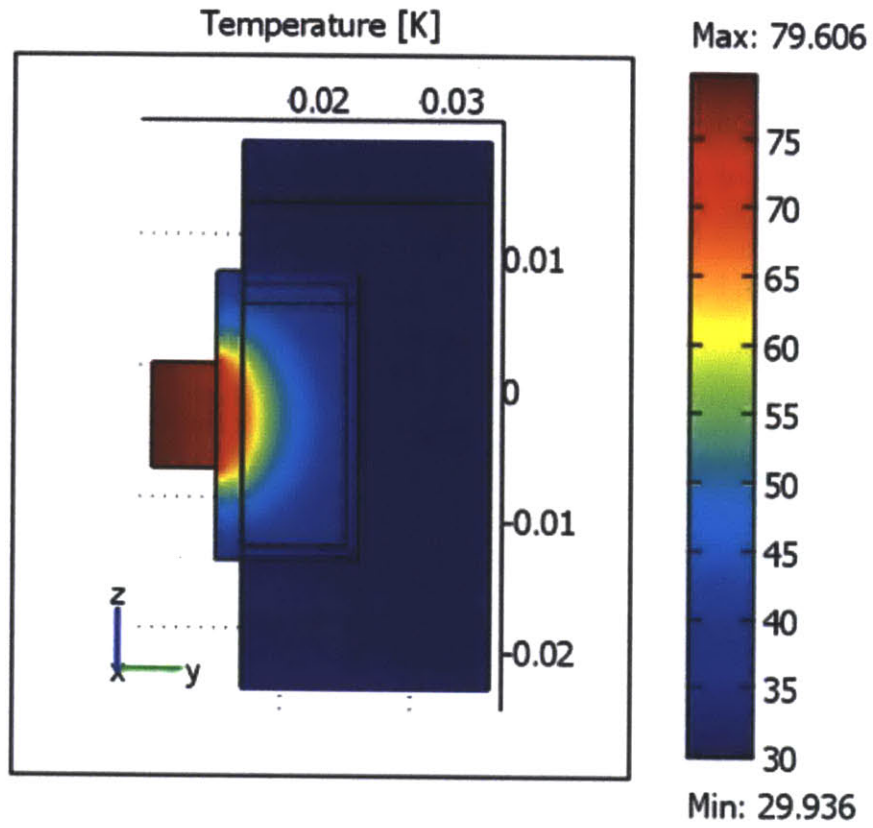
*Figure 7.1: Optimized wick temperature distribution with $\Delta T$=30 ºC and $T_{hot}$=69.5 ºC.*

# 8 References

1. Carey, V. P. Liquid-vapor Phase-change Phenomena : An Introduction to the Thermophysics of Vaporization and Condensation Processes in Heat Transfer Equipment. New York: Taylor & Francis, 2008.

2. Incropera, Frank P., Fundamentals of Heat and Mass Transfer, Frank P. Incropera, et al., Hoboken, NJ: John Wiley, c2007.

3. H.A. Kariya, C. Koveal, J. Allison, M. Kelley, M. McCarthy, J.G. Brisson, and E.N. Wang; A Capillary-pumped Loop Heat Pipe with Multi-layer Microstructured Wicks, pages 119-122, Proceedings Power MEMS, 2009

4. Lienhard, John H., A Heat Transfer Textbook. Mineola, N.Y.: Dover Publications, 2011.

5. Majumdar, Pradip. Computational Methods for Heat and Mass Transfer. New York. Taylor & Francis, 2005.

# 9 Appendix A: FDA Structure

## 9.1 Cubic Construction

Complex heat flows can be calculated by discretizing complex shapes into fundamental units. The complex flow becomes the interactions of many simple flows between the fundamental units. Finite difference matrices describe the relations between these units and can be solved to find the average temperature of each unit. The essential step in constructing a finite difference matrix is establishing the energy balances relating the fundamental units.

For the cubic finite difference matrix an element-centric nodal mesh was chosen as shown in Figure 9.1. The temperature reference is placed in the center of the mesh element instead of the corner. This simplifies the number of possible interactions between nodes where in this case, the center node only interacts with the six orthogonal neighboring nodes instead of eight neighboring nodes as in the element-corner nodal mesh. The cost of this simplification is that any material boundaries occur half of a step size away as shown in Figure 9.2, so nodes do not directly indicate boundary temperatures.
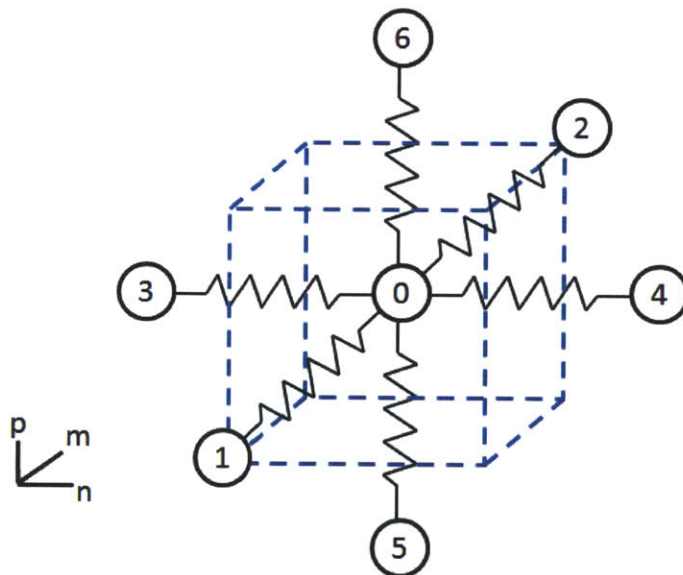


*Figure 9.1: Three dimensional mesh element of cubic finite difference matrix. Node zero indicates the node of interest and nodes one through six indicate the neighboring nodes.*
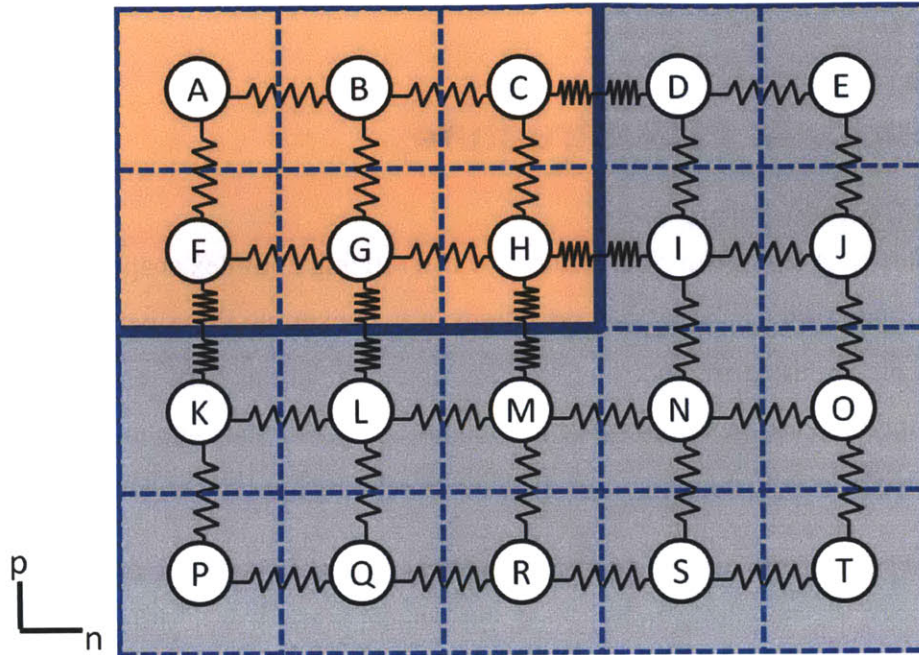
*Figure 9.2Two dimensional view of cubic mesh showing how temperature-referencing nodes relate to material boundaries for an element-centric nodal mesh. The alternative configuration places each node at the corner of mesh elements and along material boundaries.*

The interactions between each node and its neighbors must obey energy conservation laws. An energy balance must be calculated and applied to each node specific to its neighboring nodes. The equation describing the energy balance between a center node and neighboring nodes of the same material is given as

$$\sum_{i=1}^{6} \frac{KA}{t}(T_i - T_0) + q_{gen}V^3 = 0 \tag{9.1}$$

where K is the material thermal conductivity, A is the interacting area, t is the thickness, $T_i$ is the temperature of the neighboring nodes, $T_0$ is the temperature of the center node, $q_{gen}$ is the rate of heat generation and V is the volume of an element. Since each node has three equal sides of length $\Delta x$ equation (9.1) can be simplified to

$$\sum_{i=1}^{6} K\Delta x(T_i - T_0) + q_{gen}(\Delta x)^3 = 0 \tag{9.2}$$

With six different neighboring nodes each capable of representing a different material or boundary condition there are many possible nodal conditions which would require many different energy balance equations such as (9.2). To simplify these energy balances and trim the code the equations can be generalized, solved for the interactions between two nodes, and combined to yield the total energy balance. For conduction between two nodes the energy balance is given as

$$\frac{(T_i - T_0)}{\frac{\Delta x}{2K_i \Delta x^2} + \frac{\Delta x}{2K_0 \Delta x^2}} = \frac{2\Delta x K_i K_0 (T_i - T_0)}{K_i + K_0} = 0 \tag{9.3}$$

where $K_i$ and $K_0$ are the thermal conductivities of the neighbor and center nodes respectively.

For convective or insulative boundary conditions the interaction between the central node and the boundary is given by

$$hA(T_\infty - T_0) = h(\Delta x)^2 (T_\infty - T_0) = 0 \tag{9.4}$$

where $T_\infty$ is the temperature of the environment and h is the coefficient of convection which is positive for convective boundary conditions and zero for insulative boundary conditions.

For constant heat flux boundary conditions the interaction equation is given as

$$q'A = q'(\Delta x)^2 = 0 \tag{9.5}$$

where q' is the heat flux.

Upon determining all of the equations describing a particular node they are summed and like terms are grouped together and input into the finite difference matrix which will be solved to calculate the temperature at each node.

## 9.2  Cylindrical Construction

The construction of a radial finite difference matrix is the same as that of a cubic finite difference matrix except the mesh element and node interaction equations are different. Since the temperature profile in a cylinder is symmetric around the axis only a radial and axial dimension are needed to describe the heat flow and construct the finite difference matrix. A cylindrical mesh element is shown below in Figure 9.3.
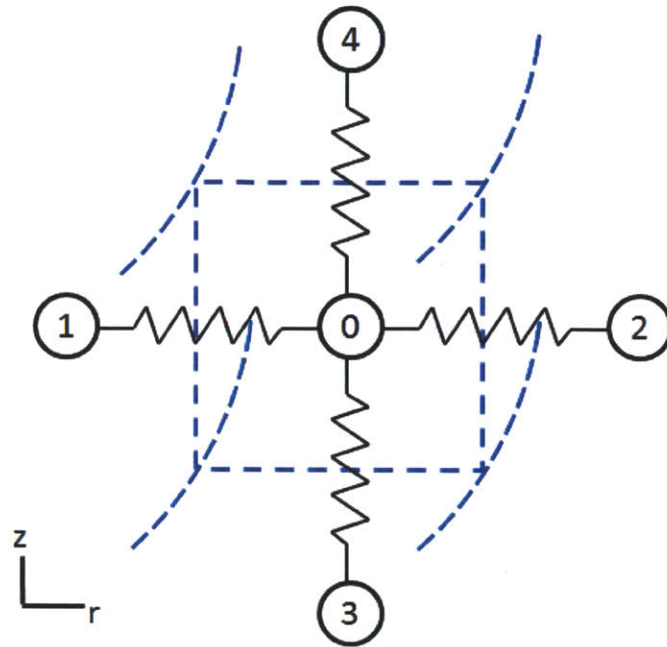
*Figure 9.3: Cylindrical node element. Curved dashed lines represent a portion of the three dimensional annulus whose thermal properties are captured by this two dimensional mesh. The dashed-line square represents the cross section of the annulus which revolves around the cylinder's axis to make the annulus mesh element.*

This cylindrical mesh construction is preferable to the cubic form when studying cylindrical geometries because it takes full advantage of symmetry and greatly reduces the number of calculations. Although this simplification makes computation easier it complicates the mesh definition as some assumptions from the cubic mesh do not hold.

The first distinction is that although the mesh is broken into even intervals along the r and z dimensions the volume and surface area of each node element increase with r. Second, since the center of mass is biased towards the outer radius of the annulus, and not at a radius averaged between the inner and outer radii, the center of mass is in a different location for each mesh element, so the effective distance between each node is different. Third, conduction in the axial dimension is takes the same form as conduction through the cubic elements but conduction through the radial dimension is described by the radial conduction equation. Therefore one must now take note of the neighboring node position when applying the generalized two-node interaction equations.

The equation for conduction along the axial dimension between nodes 1 and 0 and nodes 0 and 2 as in Figure 9.3 respectively become

$$\frac{2\pi \Delta x (T_1 - T_0)}{\left(\frac{\ln\frac{r_s}{r_1}}{K_1} + \frac{\ln\frac{r_0}{r_s}}{K_0}\right)} = 0 \qquad (9.6)$$

$$\frac{2\pi \Delta x (T_2 - T_0)}{\left(\frac{\ln\frac{r_s}{r_j}}{K_0} + \frac{\ln\frac{r_2}{r_s}}{K_2}\right)} = 0 \qquad (9.7)$$

where $r_s$ is the radius marking the boundary between interacting nodes, $r_i$ is the radius measured from the cylinder's axis to the center of mass of the node i.

The expression for conduction in the axial direction becomes

$$\frac{2A_z K_i K_0 (T_i - T_0)}{\Delta x (K_i + K_0)} = 0 \qquad (9.8)$$

where $A_z$ is the planar surface area of the central node.

# 10 Appendix B: Matlab Code

## 10.1 Dimensioner.m

*The main FDA call script, this file receives all dimensions, assembles the property matrix, calls upon the particular node construction scripts, and computes and plots the temperature profile.*

```
%%Dimensioner
%%Build 3D geometric matrix
clear all; clc; close all;

CubicFDA=0;
RadialFDA=1;
ploton=1;
drawon=1;
multiplot=0;
StepSize=0.0002; %mesh lengths

%%input geometric values here
%Materials
WaterRadial=.001;
WaterVertical=.001;
CaseRadial=.005;
CaseVertical=.005;
BasePlateHeight=.00199;
HeaterRadius=0.005;
HeaterHeight=0.007;
WickRadius=.010;
WickHeight=.010

%Dependent Radii
WaterRadius=WickRadius+WaterRadial;
BasePlateRadius=WaterRadius;
CaseRadius=WaterRadius+CaseRadial;

%Dependent Heights
CaseHeight=WickHeight+WaterVertical+CaseVertical;

%Region Index, these are the values which will indicate the nature of a
%slice of the 3D physical matrix. Geometry represented by positive
%indicies, Boundary conditions represented by negative indicies
IEmpty=0;
IHeater=1;
IBasePlate=2;
IWick=3;
IWater=4;
ICase=5;
IHeat=-1;
IAdiabatic=-2;
IConvection=-3;
```

```
qgen=0;
Rtc=0;%thermal contact resistance


%Material Properties
por=0.5; %porosity
KAl=237; %W/mK
KWater=0.6; %W/mK
KSt=43; %W/mK
KSSsolid=12; %W/mK
KSSsint=2; %W/mK
KSSwet=2; %W/mK
KValue=[KAl;
     KSSsolid;
     KSSwet;
     KWater;
     KAl];


%Build circular blocks
[CCase,nCase]=circler(CaseRadius,StepSize);
[CWater,nWater]=circler(WaterRadius,StepSize);
[CWick,nWick]=circler(WickRadius,StepSize);
[CBasePlate,nBasePlate]=circler(BasePlateRadius,StepSize);
[CHeater,nHeater]=circler(HeaterRadius,StepSize);


mnMax=nCase+2; %This is the length of the sides of the horizontal slice of
the 3D matrix
MN=zeros(mnMax,mnMax); %Basic frame slice matrix
MNones=ones(mnMax,mnMax);


%Boundary Conditions
Qin=5;%W
heat=Qin/(size(find(CHeater~=0),1)*StepSize^2*4);%calculates the heat per
unit area for the mesh approximaiton of a heated cylinder... cannot just use
1/4*pi*r^2 because the discretized area is different
adi=0;
Tinf=0; %degrees celsius
UA=.17;%W/K
h=UA/((.0*StepSize+StepSize*(nCase))^2*pi); %W/m^2K
CValue=[heat;
     adi;
     h];
Cond=[h,Qin,Tinf]';


for once=[1:1]
%Create layers from top down

%Layer 1: Convective BC above case
L1=MN;
L1(2:nCase+1,2:nCase+1)=CCase*IConvection;


%Layer 2: Adiabatic symetry; Case; Convection
L2=MNones;
L2(2:nCase+1,2:nCase+1)=L2(2:nCase+1,2:nCase+1)-CCase;
L2=L2*IAdiabatic;
```

```
L2(2:nCase+1,2:nCase+1)=L2(2:nCase+1,2:nCase+1)+CCase*ICase;


%Layer 3: Adiabatic; Water; Case; Convection
L3=L2;
CWaterNeg=-(CWater-ones(size(CWater)));
l3restore=L3(2:nWater+1,2:nWater+1).*CWaterNeg;
L3(2:nWater+1,2:nWater+1)=CWater*IWater;
L3(2:nWater+1,2:nWater+1)=L3(2:nWater+1,2:nWater+1)+l3restore;


%Layer 4: Adiabatic; Wick; Water; Case; Convection
L4=L3;
CWickNeg=-(CWick-ones(size(CWick)));
l4restore=L4(2:nWick+1,2:nWick+1).*CWickNeg;
L4(2:nWick+1,2:nWick+1)=CWick*IWick;
L4(2:nWick+1,2:nWick+1)=L4(2:nWick+1,2:nWick+1)+l4restore;


%Layer 5: Adiabatic; BasePlate; Adiabatic (Multiple)
L5=MNones*IAdiabatic;
CBasePlateNeg=-(CBasePlate-ones(size(CBasePlate)));
l5restore=L5(2:nBasePlate+1,2:nBasePlate+1).*CBasePlateNeg;
L5(2:nBasePlate+1,2:nBasePlate+1)=CBasePlate*IBasePlate;
L5(2:nBasePlate+1,2:nBasePlate+1)=L5(2:nBasePlate+1,2:nBasePlate+1)+l5restore
;


%Layer 6: Adiabatic; BasePlate; Adiabatic
L6=L5;


%Layer 7: Adiabatic; Heater; Adiabatic (Multiple)
L7=MNones*IAdiabatic;
CHeaterNeg=-(CHeater-ones(size(CHeater)));
l7restore=L7(2:nHeater+1,2:nHeater+1).*CHeaterNeg;
L7(2:nHeater+1,2:nHeater+1)=CHeater*IHeater;
L7(2:nHeater+1,2:nHeater+1)=L7(2:nHeater+1,2:nHeater+1)+l7restore;


%Layer 8: Adiabatic; Heater; Adiabatic
L8=L7;


%Layer 9: Heat
L9=MN;
L9(2:nHeater+1,2:nHeater+1)=CHeater*IHeat;
L9(L9==0)=-2;


%%Assemble 3D Matrix

M=L9;%initiates matrix with heat flux in layer
p9=1;
[M,p8]=stacker(M,L8,StepSize,HeaterHeight,1);%adds heater layers
M(:,:,size(M,3)+1)=L7;
p7=1;
[M,p6]=stacker(M,L6,StepSize,BasePlateHeight,0);%adds BasePlate layers
M(:,:,size(M,3)+1)=L5;%adds layer 5
p5=1;
[M,p4]=stacker(M,L4,StepSize,WickHeight,0);%adds wick layers
[M,p3]=stacker(M,L3,StepSize,WaterVertical,0);%adds water layers
[M,p2]=stacker(M,L2,StepSize,CaseVertical,0);%adds case layers
```

```matlab
M(:,:,size(M,3)+1)=L1;%adds convective top layer
p1=1;
end
p=[p1 p2 p3 p4 p5 p6 p7 p8 p9];%groups together the number of nodes composing
the height of each layer starting from the top

x=StepSize;%short hand
%Create Radial Property Matrix, 2D
RadialSlice=2;
sx=size(M,1);
sz=size(M,3);
Mr=zeros(sz,sx);
for i=1:sz
    Mr(i,:)=M(RadialSlice,:,i);
end
%calculate radii and areas of each node
rNodes=size(Mr,2)-1;
ri=StepSize*(2*[1:rNodes]-1)/2;%radius of each node
rci=sqrt(ri.^2+(StepSize^2)/4);%calculate the location of each centroid
Az=2*pi*ri*StepSize;%area of vertical conduction
Ar=[0,2*pi*StepSize*(ri+StepSize)];%area of radial conduction, begining with
zero

CValuer=[Qin;
    adi;
    h];
Ah=sum(Az(1:nHeater));

if CubicFDA==1
    [T,I]=fCubicFDA(M,StepSize,KValue,CValue,x,Rtc,Tinf,qgen);
end
if RadialFDA==1
    [Tr,Ir]=fRadialFDA(Mr,StepSize,KValue,CValuer,ri,Ar,Az,x,Rtc,Tinf,Ah);
end

%Map to 3D grid
if CubicFDA==1
TM=I;
for i=1:prod(size(I))
    if TM(i)>0
        TM(i)=T(TM(i));
    else
        TM(i)=0;
    end
end
end

if RadialFDA==1
TMr=Ir;
for i=1:prod(size(Ir))
    if TMr(i)>0
        TMr(i)=Tr(TMr(i));
    else
        TMr(i)=0;
    end
end
end
```

```
end


%Pull out critical temperatures
%get the critical nodes
nWickBase=sum(p(5:8))+2;
nWickTop=sum(p(4:8))+2;
nWickRadius=nWick+1;
nTopSurface=size(M,3)-1;
nEdgeSurface=size(M,2)-2;

%find temperature at critical nodes
%Cubic
if CubicFDA==1
Th_C=TM(2,2,nWickBase);
Twz_C=TM(2,2,nWickTop);
Twr_C=TM(2,nWickRadius,nWickBase);
TsurfaceCenter_C=TM(2,2,nTopSurface);
TsurfaceEdge_C=TM(2,nEdgeSurface,nTopSurface);
gTemps(1:5)=[Th_C,Twz_C,Twr_C,TsurfaceCenter_C,TsurfaceEdge_C];
dtCr=Th_C-Twr_C
dtCz=Th_C-Twz_C
end


%Radial
if RadialFDA==1
Th_R=TMr(nWickBase,2);
Twz_R=TMr(nWickTop,2);
Twr_R=TMr(nWickBase,nWickRadius);
TsurfaceCenter_R=TMr(nTopSurface,2);
TsurfaceEdge_R=TMr(nTopSurface,nEdgeSurface);
gTemps(6:10)=[Th_R,Twz_R,Twr_R,TsurfaceCenter_R,TsurfaceEdge_R];
dtRr=Th_R-Twr_R;
dtRz=Th_R-Twz_R;
end



%Temperature Processing
if CubicFDA==1
Tratio_C=Twz_C/Twr_C;
Tdrop_C=Th_C-max([Twz_C,Twr_C]);
end

if RadialFDA==1
Tratio_R=Twz_R/Twr_R;
Tdrop_R=Th_R-max(Twz_R,Twr_R);
end

%%%Plotting
if CubicFDA==1
sliceH=nWickBase;
sliceV=2;
sx=size(TM,1);
sz=size(TM,3);
TMy=zeros(sz,sx);
```

```
for i=1:sz
    TMy(i,:)=TM(sliceV,:,i);
end
end

if ploton==1
    if CubicFDA==1 & RadialFDA==1
subplot 221
surface(TM((2:end),(2:end),sliceH));colorbar
set(gca,'DataAspectRatio',[1 1 1])
subplot 222
surface(TMy((5:end),(2:end-3)));colorbar
set(gca,'DataAspectRatio',[1 1 1])
subplot 223
surface(TMr((2:end),(2:end)));colorbar
set(gca,'DataAspectRatio',[1 1 1])
subplot 224
surface(TMr((5:end),(2:end-3)));colorbar
set(gca,'DataAspectRatio',[1 1 1])
    end

if RadialFDA==1

figure;
cont1=contourf(TMr((3:end),(2:end)),[min(TMr(TMr~=0)):5:max(max((TMr)))]);
colorbar
set(gca,'DataAspectRatio',[1 1 1])
set(gca,'YTickLabelMode','manual','XTickLabelMode','manual')
ytick=get(gca,'YTick');
xtick=get(gca,'XTick');
set(gca,'XTickLabel',xtick*StepSize,'YTickLabel',ytick*StepSize)
xlabel('Radial Dimension, [m]')
ylabel('Axial Dimension, [m]')


hold on
lw=3; %linewidth
plot([0,0],[0,sum(p(2:8))],'k','LineWidth', lw)
plot([0,nHeater],[0,0],'k','LineWidth', lw)
plot([0,nBasePlate],[p8+p7,p8+p7],'k','LineWidth', lw)
plot([0,nCase],[sum(p(5:8)),sum(p(5:8))],'k','LineWidth', lw)
plot([0,nWick],[sum(p(4:8)),sum(p(4:8))],'k','LineWidth', lw)
plot([0,nWater],[sum(p(3:8)),sum(p(3:8))],'k','LineWidth', lw)
plot([nWick,nWick],[sum(p(5:8)),sum(p(4:8))],'k','LineWidth', lw)
plot([nWater,nWater],[sum(p(7:8)),sum(p(3:8))],'k','LineWidth', lw)
plot([nCase,nCase],[sum(p(5:8)),sum(p(2:8))-1],'k','LineWidth', lw)
plot([nHeater,nHeater],[0,sum(p(8:9))],'k','LineWidth', lw)
plot([0,nCase],[sum(p(2:8))-1,sum(p(2:8))-1],'k','LineWidth', lw)
end
end
```

## 10.2 fCubicFDA.m

*A rectangular node structure script, this script applies the rectangular node interaction structure to each node.*

```
function [T,I]=fCubicFDA(M,StepSize,KValue,CValue,x,Rtc,Tinf,qgen);


%CUBIC
%Create Index Matrix and Reference List
%for 3D Cubic
I=zeros(size(M));%frame for Index matrix
[xx,yy,zz]=size(M);
NodeCount=0;%start counter at 0
for k=1:zz
    for j=1:yy
        for i=1:xx
            NodeType=M(i,j,k);
            if NodeType>0
                NodeCount=NodeCount+1; %keep running count
                I(i,j,k)=NodeCount; %input index into Index matrix
                NodeReference(NodeCount)=NodeType;%makes a list of node types
ordered as they appear
            end
        end
    end
end



%Create Neighbor matrix, collect neighbor information
%For 3D Cubic
NeighborIndicies=zeros(NodeCount,6);%create frame for neighbor matrix
NeighborValues=zeros(NodeCount,6);
nc2=0; %node counter
for k=1:zz
    for j=1:yy
        for i=1:xx
            if I(i,j,k)~=0
                nc2=nc2+1;
                NeighborIndexOne=[I(i-1,j,k),I(i+1,j,k),I(i,j-
1,k),I(i,j+1,k),I(i,j,k-1),I(i,j,k+1)];
                NeighborValueOne=[M(i-1,j,k),M(i+1,j,k),M(i,j-
1,k),M(i,j+1,k),M(i,j,k-1),M(i,j,k+1)];
                NeighborIndicies(nc2,:)=NeighborIndexOne;
                NeighborValues(nc2,:)=NeighborValueOne;
            end
        end
    end
end



%Node Collection and Standardization
%For 3D Cubic
%Put together matrix containing node indicies and BC names
NIndex=NeighborIndicies;
zs=find(NIndex==0);%this is the case where there is not a material node, just
a boundary condition, therefore no neighbor index
NIndex(zs)=NeighborValues(zs);

%Put together matrix containing only neighbor node properties or BCs
NProp=NIndex;
```

```
zpos=find(NIndex>0);%note, all BCs are less than 1, only indicies are greater
than 1
NProp(zpos)=NodeReference(NProp(zpos));

%Create normalized property matrix
NPropNorm=NProp;
for i=1:NodeCount
    count=0;
    comp=zeros(1:6);%6 is the number of columns in the NPropNorm matrix
    for j=1:6
        if NPropNorm(i,j)<0
            if NPropNorm(i,j)==-3%merge adiabatic with convection
                NPropNorm(i,j)=-2;
            end
            NPropNorm(i,j)=NPropNorm(i,j)+10;
        elseif NPropNorm(i,j)>0%these lines normalize materials
            b=find(comp==NPropNorm(i,j));
            if isempty(b)==1
                count=count+1;
                comp(count)=NPropNorm(i,j);
                NPropNorm(i,j)=count;
            else
                NPropNorm(i,j)=b;
            end
        elseif NPropNorm(i,j)==0
            NPropNorm(i,j)=8;
        end
    end
end
NPropNormCol=NPropNorm*[10^5;10^4;10^3;10^2;10^1;10^0];
NPropNormColS=sort(NPropNorm,2)*[10^5;10^4;10^3;10^2;10^1;10^0];

KI=zeros(NodeCount,3);%keep track of materials, max of three different kinds
%internal nodes
UniqueCon=unique(NPropNormColS);
nUniqueCon=size(UniqueCon);

%Assemble Final Matrix
%For 3D Cubic
FDM=sparse([],[],[],NodeCount,NodeCount,NodeCount*7);
FDA=zeros(NodeCount,1);
OppNode=[2 1 4 3 6 5];%gives node opposite to index position
nCheck=0;%counter to keep track of how many nodes have been treated

for i=1:NodeCount %Loop over each node
        m1=NodeReference(i);
        K1=KValue(m1);
        n16=zeros(6,5);
        for j=1:6
            n16(j,1)=NProp(i,j);
            if NProp(i,j)>0 %dealing with material node
                if NProp(i,j)==m1 %same material
                    n16(j,2)=K1*x;
                    n16(j,3)=-K1*x;
                    n16(j,4)=0;
                else %different material
```

61

```
                        Kj=KValue(NProp(i,j));
                        n16(j,2)=1/(1/(2*K1*x)+Rtc+1/(2*Kj*x));
                        n16(j,3)=-1/(1/(2*K1*x)+Rtc+1/(2*Kj*x));
                        n16(j,4)=0;
                    end
            else %Deals with Boundary condition
                    cjpos=j;
                    cj=-NProp(i,cjpos);
                    Cj=CValue(cj);
                    if NProp(i,j)==-1 %Heat Conduction
                        n16(j,2)=0;
                        n16(j,3)=0;
                        n16(j,4)=Cj*x^2;
                    else %adiabatic/convection case
                        n16(j,2)=0;
                        n16(j,3)=-Cj*x^2;
                        n16(j,4)=Cj*x^2*Tinf;
                    end
            end
            n16(j,5)=NeighborIndicies(i,j);
        end
        nonzeros=find(n16(:,5)~=0);
        FDM(i,n16(nonzeros,5))=n16(nonzeros,2);
        FDM(i,i)=sum(n16(:,3));
        FDA(i)=-sum(n16(:,4))-qgen*x^3;
        nCheck=nCheck+1;
end


%%Calculate Temperatures
T=FDM\FDA;


## 10.3 fRadialFDA.m

*A radial node structure script, this script applies the radial node interaction structure
to each node.*


function
[Tr,Ir]=fRadialFDA(Mr,StepSize,KValue,CValuer,ri,Ar,Az,x,Rtc,Tinf,Ah)

%RADIAL

%for 2D Radial
Ir=zeros(size(Mr));%frame for Index matrix
[xx,yy]=size(Mr);
NodeCountr=0;%start counter at 0
for j=1:yy
    for i=1:xx
        NodeType=Mr(i,j);
        if NodeType>0
            NodeCountr=NodeCountr+1; %keep running count
            Ir(i,j)=NodeCountr; %input index into Index matrix
```

```
                NodeReferencer(NodeCountr)=NodeType;%makes a list of node types
ordered as they appear
                NodeRadiusIndex(NodeCountr)=j-1;%records the radial node position
of each node begining with the first material node indexed as 1
        end
    end
end


%for 2D Radial
NeighborIndiciesr=zeros(NodeCountr,4);%create frame for neighbor matrix
NeighborValuesr=zeros(NodeCountr,4);
nc2r=0; %node counter
for j=1:yy
    for i=1:xx
        if Ir(i,j)~=0
            nc2r=nc2r+1;
            NeighborIndexOner=[Ir(i,j-1),Ir(i,j+1),Ir(i-1,j),Ir(i+1,j)];
            NeighborValueOner=[Mr(i,j-1),Mr(i,j+1),Mr(i-1,j),Mr(i+1,j)];
            NeighborIndiciesr(nc2r,:)=NeighborIndexOner;
            NeighborValuesr(nc2r,:)=NeighborValueOner;
        end
    end
end


%For 2D Radial
%Put together matrix containing node indicies and BC names
NIndexr=NeighborIndiciesr;
zsr=find(NIndexr==0);%this is the case where there is not a material node,
just a boundary condition, therefore no neighbor index
NIndexr(zsr)=NeighborValuesr(zsr);

%Put together matrix containing only neighbor node properties or BCs
NPropr=NIndexr;
zposr=find(NIndexr>0);%note, all BCs are less than 1, only indicies are
greater than 1
NPropr(zposr)=NodeReferencer(NPropr(zposr));

%Create normalized property matrix
NPropNormr=NPropr;
for i=1:NodeCountr
    countr=0;
    compr=zeros(1:4);%4 is the number of columns in the NPropNorm matrix
    for j=1:4
        if NPropNormr(i,j)<0
            if NPropNormr(i,j)==-3%merge adiabatic with convection
                NPropNormr(i,j)=-2;
            end
            NPropNormr(i,j)=NPropNormr(i,j)+10;
        elseif NPropNormr(i,j)>0%these lines normalize materials
            br=find(compr==NPropNormr(i,j));
            if isempty(br)==1
                countr=countr+1;
                compr(countr)=NPropNormr(i,j);
                NPropNormr(i,j)=countr;
            else
                NPropNormr(i,j)=br;
```

63

```
                    end
            elseif NPropNormr(i,j)==0
                    NPropNormr(i,j)=8;
            end
        end
end
NPropNormColr=NPropNormr*[10^3;10^2;10^1;10^0];
NPropNormColSr=sort(NPropNormr,2)*[10^3;10^2;10^1;10^0];



%For 2D Radial
FDMr=sparse([],[],[],NodeCountr,NodeCountr,NodeCountr*5);
FDAr=zeros(NodeCountr,1);
OppNoder=[2 1 4 3];%gives node opposite to index position
nCheckr=0;%counter to keep track of how many nodes have been treated

for i=1:NodeCountr
    m1=NodeReferencer(i);
    K1=KValue(m1);
    r0n=NodeRadiusIndex(i);%gives index of the node radial position
    r0=ri(r0n);%gives value of the node radial position
    A1=Ar(r0n);%gives the smaller radial area
    A2=Ar(r0n+1);%gives the larger radial area
    A34=Az(r0n);%gives the flat area of vertical conduction
    n16=zeros(4,5);%column data:1-NodeProperty, 2-T(j) Multiplier, 3-To
Multiplier, 4-Constant T Multiplier, 5-Neighbor Index
    for j=1:4%sweep over each of the neighboring nodes
        n16(j,1)=NPropr(i,j);
        if j==1
            if r0n==1
                n16(j,2)=0;
                n16(j,3)=0;
                n16(j,4)=0;
            else
                if NPropr(i,j)>0 %dealing with material node

                    if NPropr(i,j)==m1 %same material
                        n16(j,2)=2*K1*pi*x/log((r0)/(r0-x));
                        n16(j,3)=-2*K1*pi*x/log((r0)/(r0-x));
                        n16(j,4)=0;
                    else %different material
                        Kj=KValue(NPropr(i,j));
                        n16(j,2)=1/(log((r0-x/2)/(r0-
x))/(2*K1*pi*x)+Rtc+log((r0+x)/(r0-x/2))/(2*Kj*pi*x));
                        n16(j,3)=-1/(log((r0-x/2)/(r0-
x))/(2*K1*pi*x)+Rtc+log((r0+x)/(r0-x/2))/(2*Kj*pi*x));
                        n16(j,4)=0;
                    end
                else %Deals with Boundary condition
                    cjpos=j;
                    cj=-NPropr(i,cjpos);
                    Cj=CValuer(cj);
                    if NPropr(i,j)==-1 %Heat Conduction
                        n16(j,2)=0;
                        n16(j,3)=0;
                        n16(j,4)=Cj*A1/Ah;
```

64

```
            else %adiabatic/convection case
                n16(j,2)=0;
                n16(j,3)=-Cj*A1;
                n16(j,4)=Cj*A1*Tinf;
            end
        end
    end
elseif j==2
    if NPropr(i,j)>0 %dealing with material node
        if NPropr(i,j)==m1 %same material
            n16(j,2)=2*K1*pi*x/log((r0+x)/(r0));
            n16(j,3)=-2*K1*pi*x/log((r0+x)/(r0));
            n16(j,4)=0;
        else %different material
            Kj=KValue(NPropr(i,j));

n16(j,2)=1/(log((r0+x/2)/(r0))/(2*Kj*pi*x)+Rtc+log((r0+x)/(r0+x/2))/(2*K1*pi*
x));%%%%%%%
            n16(j,3)=-
1/(log((r0+x/2)/(r0))/(2*Kj*pi*x)+Rtc+log((r0+x)/(r0+x/2))/(2*K1*pi*x));
            n16(j,4)=0;
        end
    else %Deals with Boundary condition
        cjpos=j;
        cj=-NPropr(i,cjpos);
        Cj=CValuer(cj);
        if NPropr(i,j)==-1 %Heat Conduction
            n16(j,2)=0;
            n16(j,3)=0;
            n16(j,4)=Cj*A2/Ah;
        else %adiabatic/convection case
            n16(j,2)=0;
            n16(j,3)=-Cj*A2;
            n16(j,4)=Cj*A2*Tinf;
        end
    end
else
    if NPropr(i,j)>0 %dealing with material node
        if NPropr(i,j)==m1 %same material
            n16(j,2)=K1*A34/x;
            n16(j,3)=-K1*A34/x;
            n16(j,4)=0;
        else %different material
            Kj=KValue(NPropr(i,j));

n16(j,2)=2*A34*(K1*Kj)/((K1+Kj)*x);%1/(1/(2*K1*A34/x)+Rtc+1/(2*Kj*A34/x));
            n16(j,3)=-2*A34*(K1*Kj)/((K1+Kj)*x);%-
1/(1/(2*K1*A34/x)+Rtc+1/(2*Kj*A34/x));
            n16(j,4)=0;
        end
    else %Deals with Boundary condition
        cjpos=j;
        cj=-NPropr(i,cjpos);
        Cj=CValuer(cj);
        if NPropr(i,j)==-1 %Heat Conduction
            n16(j,2)=0;
            n16(j,3)=0;
```

```
                    n16(j,4)=Cj*A34/Ah;
                else %adiabatic/convection case
                    n16(j,2)=0;
                    n16(j,3)=-Cj*A34;
                    n16(j,4)=Cj*A34*Tinf;
                end
            end
        end
    n16(j,5)=NeighborIndiciesr(i,j);
    end
    nonzeros=find(n16(:,5)~=0); %find neighbors
    FDMr(i,n16(nonzeros,5))=n16(nonzeros,2);
    FDMr(i,i)=sum(n16(:,3));
    FDAr(i)=-sum(n16(:,4));%not considering heat generation for now
    nCheckr=nCheckr+1;
end

%%Calculate Temperatures
Tr=FDMr\FDAr;
```

## 10.4 cicler.m

*A script to discretize circles for the construction of layers.*

```
function [M,n]=circler(R,dx);
%make a circle from input radius, output Matrix and max 1D dimension
%Circle descritizer,

PropNum=1; %region identifier, set as 1 for generic function

n=round(R/dx); %descritize radius, max points in a 1D radius
M=zeros(n,n); %establish matrix

for i=1:n
    for j=1:n
        if ((i*dx)^2+(j*dx)^2)^.5 <= R+dx/2
            M(i,j)=PropNum; %distinguish included cells
        end
    end
end
 error=.25*pi*R^2-sum(sum(M))*dx^2;
end
```

## 10.5 stacker.m

*A script which compiles property layers to make 3D property matrix.*

```
function [Mnew,p]=stacker(M,L,dx,h,ExtraLayers)
%puts vertical dimension into the geometry matrix

p=floor(h/dx)-ExtraLayers;%how many times does the layer repeat. Some
material elements are also represented by boundary condition layers
Mnew=M;
for i=1:p
    Mnew(:,:,size(Mnew,3)+1)=L;
end
end
```

# 11 Appendix C: Cooling System Design

A simple way to cool the nucleation device is by flowing water through pipes soldered onto the top surface. An effective heat transfer coefficient for the top can be calculated by scaling the overall heat transfer coefficient of the piping system to the area of the top of the device. This effective heat transfer coefficient enters into the thermal model as the coefficient of convection on the top surface of the case.

The first step is to find the heat transfer coefficient into the pipes. For laminar flow this is given by the Nusselt correlations.

$$Nu_D = 4.36, \quad q_s" = constant \tag{11.1}$$

$$Nu_D = 3.66, \quad T_s = constant \tag{11.2}$$

Since aluminum is highly conductive the temperature across the surface of the case will be approximately constant for the low heat inputs expected of the system so the Nusselt number can be taken as 3.66. This assumption can be verified after calculating the heat transfer coefficient. If the Biot number is significantly less than 1 it is reasonable to say that the surface has a constant temperature.

With the formula for the Nusselt number below

$$Nu_D = \frac{hD}{k} \tag{11.3}$$

Where h is the average heat transfer coefficient, D is the diameter of the pipe, and k is the conductivity of the fluid flowing through the pipe. Equations 11.1 and 11.3 solve for the average heat transfer coefficient into the pipe, $h_p$.

The heat transfer coefficient between the water and the pipes can be scaled to the heat transfer coefficient between the device and the pipes by comparing the area of contact between the water and heated surface to that between the device and the cooling system.

$$UA = h_p A_p = h_d A_d \tag{11.4}$$

Thus the heat transfer coefficient depends entirely on geometry. For the purposes of design optimization the piping system was structured in a scalable form as shown in Figure 11.1 below.
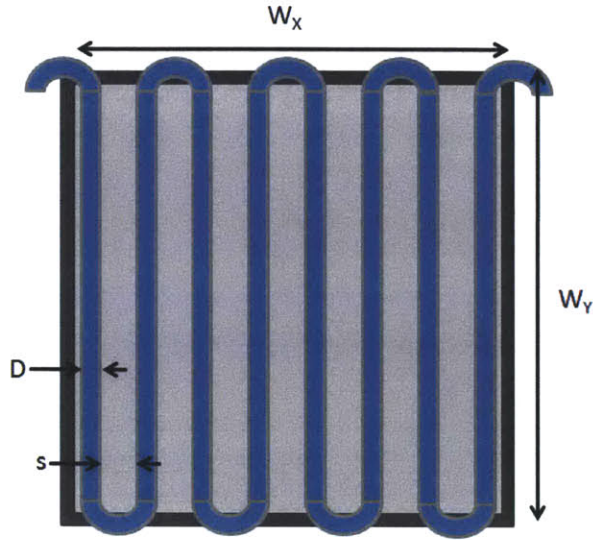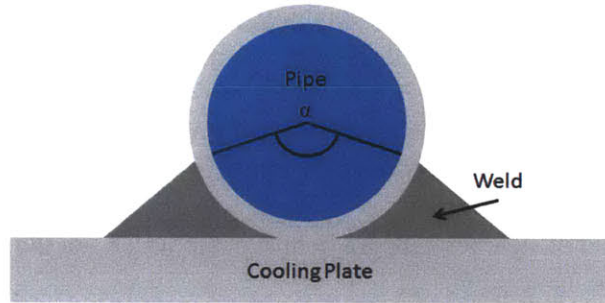
Figure 11.1: Top view of the scaleable cooling unit.



Figure 11.2: Cross-section of pipe.

$A_p$, the area of the pipe at the temperature of the heated surface, is scaled by the factor $\alpha$ because only part of the perimeter of the pipe is in good contact with the surface through the weld. $A_p$ is given as

$$A_p = \pi \alpha D L \tag{11.5}$$

$$L = 2nW_x \tag{11.6}$$

$$n = \frac{W_y}{2(D+s)} \tag{11.7}$$

The area of the device in contact with the cooling system, $A_d$, will vary during the wick optimization process. Instead of fixing the convection coefficient, $h_d$, UA was fixed and $h_d$ was updated as the area of the top surface changed. This way the cooling system and the wick can be designed independently. Another benefit of this decoupling is if the area of the device is too small or the pipes are

getting poor contact with the heated surface the UA can be made as large as desired by creating independent cooling units which sit on top of the device and are thick enough to diffuse the heat evenly across the surface as in Figure 11.3.
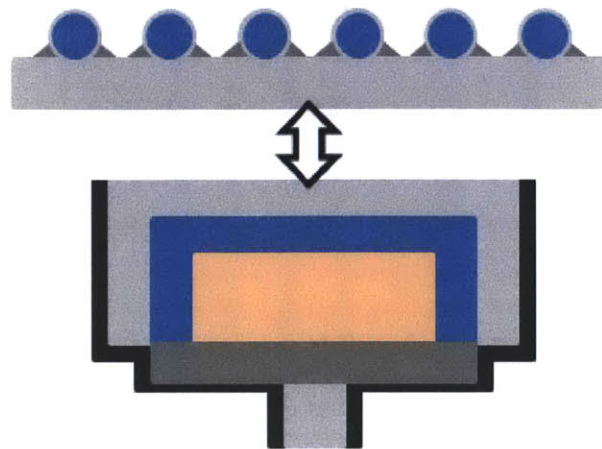


*Figure 11.3: Interchangeable cooling unit.*

For reasonable values: D=1.5 cm, s=1 cm, $\alpha$ =0.5, and $W_x=W_y=1$ cm, UA is 1.38 W/K and $h_d$ is 138 W/m$^2$K. To verify the constant temperature condition the Biot number is calculated by

$$Bi = \frac{hL}{K_s} \tag{11.8}$$

where Ks is the conductivity of the solid (aluminum), and $K_s$=237 W/mK. Let L, the characteristic length, be 1 cm. The Biot number for the heat transfer coefficient between the water and the pipe is 0.0058, much less than 1. This indicates that the temperature gradient is in the water, not the heated surface, so the temperature is essentially constant.